MODE I FRACTURE CRITERION AND THE FINITE-WIDTH CORRECTION FACTOR FOR NOTCHED LAMINATED COMPOSITES

By

BOKWON LEE

A THESIS PRESENTED TO THE GRADUATE SCHOOL
OF THE UNIVERSITY OF FLORIDA IN PARTIAL FULFILLMENT
OF THE REQUIREMENTS FOR THE DEGREE OF
MASTER OF SCIENCE

UNIVERSITY OF FLORIDA

2003

To my parents, Jonghan Lee and Jongok Woo

ACKNOWLEDGMENTS

I am grateful to Dr. Bhavani V. Sankar for giving me the opportunity of pursuing this research and for the insightful guidance he provided me, not only in the research work, but throughout the course of my graduate studies at the University of Florida. I would also like to express my gratitude to Dr. Peter G. Ifju and Dr. Ashok V. Kumar for serving as my supervisory committee members and for giving me advice.

I must also acknowledge the Korea Airforce for giving me an opportunity to study abroad and meet wonderful people in the research world. The experience I have gained at the Center for Advanced Composites will be greatly helpful to me in my duties as an Airforce Logistics Officer.

I wish to thank all my fellow students for the fun and support. I greatly look forward to having all of them as colleagues in the years ahead.

The final acknowledgement goes to all of my family, Jonghan Lee, Jongok Woo, and Hongwon Lee, for their unconditional support and love.

TABLE OF CONTENTS

page

LIST OF TABLES

LIST OF FIGURES

Abstract of Thesis Presented to the Graduate School
of the University of Florida in Partial Fulfillment of the
Requirements for the Degree of Master of Science

MODE I FRACTURE CRITERION AND THE FINITE-WIDTH CORRECTION FACTOR FOR NOTCHED LAMINATED COMPOSITES

By

Bokwon Lee

August 2003

Chair: Bhavani V. Sankar
Major Department: Mechanical and Aerospace Engineering

The purpose of this study was to investigate the applicability of the existing lay-up independent fracture criterion for notched composite laminates. A detailed finite element analysis of notched graphite/epoxy laminates was performed to understand the nature of stresses and crack tip parameters in finite-width composite panels. A new laminate parameter b has been identified which plays a crucial role in the fracture of laminated composites. An empirical formula has been developed for finite-width correction factors for composite laminates in terms of crack length to panel width ratio and b. The effects of blunt crack tip and local damage on fracture behavior of notched composite laminates are investigated using the FE analysis. The results of experiments performed elsewhere are analyzed in the light of new understanding of crack tip stresses, and the applicability of the lay-up independent fracture criterion for notched composite laminates is discussed. It is determined that the analytical lay-up independent fracture

model that considers local damage effect provides good correlation with experimental data, and the use of orthotropic finite-width correction factor improves the accuracy of notched strength prediction of composite laminates.

CHAPTER 1
INTRODUCTION

1.1 Background and Objectives

Composite laminates are widely used in aerospace, automobile and marine industries. Because of their high strength-to-weight and stiffness-to-weight ratio, use of fiber-reinforced composite materials in advanced engineering structures such as high-performance aircraft has been increasing. Recently, laminated composites have been increasingly used in military fighter airframes and external surfaces because those designs are required to handle high aerodynamic forces, be lightweight for maximizing air-to-air performance, minimize radar cross section, and withstand foreign object and battle damage. In addition, by properly sequencing the stacking lay-up, a wide range of design requirements can be met. Laminated composites posses distinctive advantages as mentioned above; however, fiber-reinforced composites exhibit notch sensitivity, and this can be an important factor in determining safe design. The problem of predicting the notched strength of laminated composites has been the subject of extensive research in the past few years. Owing to the inherent complexity and the number of factors involved in their fracture behavior, several semi-empirical failure criteria have been proposed and have gained popularity. Some failure criteria are based on concepts of linear-elastic fracture mechanics (LEFM), while others are based on the characteristic length and stress distribution in the vicinity of the notch. In general, these models rely on a curve-fitting procedure for the determination of a number of material and laminate parameters, involving testing of notched and unnotched specimens for each selected lay-up.

One limitation commonly reported is that the fracture toughness in many cases is dependent upon laminate configuration, the specific fiber/matrix system, etc. The use of these failure criteria without properly accounting for this dependence has led to some mixed results. Awerbuch and Madhukar [1] reviewed some of the most commonly used fracture criteria for notched laminated composites. They collected data from several sources and different materials and evaluated the performance of each criterion. They concluded that the parameters are strongly dependent on laminate configuration and material system and must be determined experimentally for each new material system and laminate configuration. To overcome this limitation of those popular failure criteria, recently a lay-up independent fracture criterion was developed by employing linear-elastic fracture mechanics concepts. The fracture toughness of the load-carrying ply in the presence of fiber breakage was considered as the principal fracture parameter.

The main objective of this research was to further verify and also improve the existing lay-up independent fracture criterion for notched laminated composites. Detailed finite element analyses, both 2D and 3D, of the laminate were performed to understand the average laminate stresses as well as stresses in individual layers. An analytical model for determining the principal fracture parameter, fracture toughness of the load-carrying ply, was also developed. It has been found that factors such as crack bluntness, local damage such as fiber splitting, delamination, etc. in the vicinity of crack tip play a significant role in reducing the stresses in angle plies and thus increasing the stresses and stress intensity factor in the load-carrying ply. A new laminate parameter, referred to as b, has been identified. This parameter represents the ratio of the axial and normal stresses at points straight ahead of crack tip, and plays a crucial role in the failure of the

notched laminate.

A secondary objective was to develop a semi-empirical solution for finite-width correction factor (FWC) for laminated composites to improve the accuracy of prediction of notched strength. Due to the lack of a closed form solution for orthotropic finite-width correction factor, most existing failure criterion used the isotropic finite-width correction factor for prediction of notched strength of laminates. In some cases, the application of the isotropic finite-width correction factors to estimate the anisotropic or orthotropic finite-width correction factors can cause significant error. An attempt was made to reduce the error in predicting the notched strength by developing an orthotropic finite-width correction factor for various laminates configurations.

1.2 Literature Review

Numerous failure models have been developed for the prediction of the notched strengths of composite laminates. Due to the complication of analyzing the fracture behavior of notched composite laminates, a number of assumptions and approximations were contained in most commonly used failure models to predict the tensile strengths of notched composite laminates. In recent years several simplified fracture models have been proposed. The scope of this research was limited to laminated composites containing a straight center crack when subjected to uniaxial tensile loading.

Waddoups, Eisenmann, and Kaminkski (WEK-LEFM models) [2] applied Linear Elastic Fracture Mechanics to composites. Their approach was to treat the local damage zone as a crack, and apply fracture mechanics. Whitney and Nuismer [3] proposed the stress-failure models. These models named the Average-Stress Criterion (ASC) and the Point-Stress Criterion (PSC) assumed that fracture occurs when the point stress or the

average stress over some characteristic distance away from the discontinuity is equal to the ultimate strength of the unnotched laminate. The characteristic distances in point stress criterion and average-stress criterion, are considered to be material constants and the evaluation of the notched tensile strength is based on the closed form expressions of the stress distribution adjacent to the circular hole. Tan [4] extended this concept and developed more general failure models, the Point Strength Model (PSM) and Minimum Strength Model (MSM). These models successfully used to predict the notched strength of composite laminates subjected to various loading conditions. Such models using a characteristic length concept have been widely used to predict ultimate strength in the presence of notches. The main disadvantage is that the characteristic length is not a material constant and depends on factors such as the lay-up configuration, the geometry of the notch, etc. Therefore, the characteristic length obtained from tests on one laminate configuration may not be extrapolated to predict the failure of other laminates of the same material system. Mar and Lin [5] proposed LEFM fracture model called Mar-Lin criterion, the damage zone model, and the damage zone criterion. They assumed that the laminate fracture must occur through the propagation of a crack lying in matrix material at the matrix/filament interface. It was able to provide good correlation with experimental data and at the same time is very simple to apply. However, the fracture parameter, which was used in Mar-Lin criterion, depends on the laminate lay-up configuration. Therefore, the application of this fracture criterion requires experimental determination of the fracture parameter for each laminate. Chang and Chang [6] and Tan [7] proposed progressive damage models which were developed to predict the extent of damage and damage progression, respectively, in notched composite laminates. The models accounted

for the reduced stress concentration associated with mechanisms of damage growth at a notch tip by reducing local laminate stiffness.

Past experimental investigations, which were carried out by Poe [8], have revealed that fiber failure in the principal load-carrying plies governs the failure of notched laminated composites. Poe and Sova [8, 9] proposed a general fracture-toughness parameter, critical strain intensity factor, which is independent of laminate orientation. This parameter was derived on the basis of fiber failure of the principal load-carrying ply and it is proportional to the critical stress intensity factor. Such an idea was adopted by Kageyama [10] who estimated the fracture toughness of the load-carrying ply by three dimensional finite element analysis. Such analyses led to lay-up independent fracture criteria based on the failure mechanism of the load-carrying ply, which governs the failure of entire laminate. Recently, Sun et al. [11, 12] proposed a new lay-up independent fracture criterion for composites containing center cracks. In their analysis, the fracture toughness of the load-carrying ply was introduced as the material parameter. Such an analysis is approximate, since it does not take into account any stress redistribution caused by local damage and it used the isotropic form factor instead of an orthotropic finite-width correction factor to account for finite width of the laminated specimens.

There are several analytical and numerical methods [13-15] to determine the orthotropic finite-width correction factor including the boundary integral equation, finite element analysis, modification of isotropic finite-width correction factor, etc. However, no closed form solutions are available. Therefore, the closed form solution for isotropic materials is frequently used for orthotropic material as well.

Current study aims to further verify the lay-up independent model including new fracture parameter and improve the accuracy for the notched strength prediction of composite laminates by using orthotropic finite-width correction factor.

Chapter 1 provides an introduction and a literature review of fracture models for notched laminated composites. Chapter 2 describes a general concept of the lay-up independent fracture model and the analytical derivation of the stress intensity factor in the load-carrying ply. Chapter 3 describes a FE modeling procedure including damage modeling and the development of the orthotropic finite-width correction factor based on FE analysis. Conclusions and some recommendations for future work are presented in Chapter 4.

CHAPTER 2
LAY-UP INDEPENDENT FRACTURE CRITERION

2.1 Introduction

Fibrous composite materials have high strength and stiffness as mentioned before. Under tension loading, however, most advanced laminated composites are severely weakened by notches or by fiber damage. Thus, a designer needs to know the fracture toughness of composite laminates in order to design damage tolerant structures. The fracture toughness of composite laminates depends on material property and laminates configuration. Consequently, testing to determine fracture toughness for each possible laminate configuration would be expensive and time-consuming work. Thus, a single fracture parameter can be used to predict fracture toughness for all laminates configurations of the same material system. Poe and Sova [8, 9] proposed a general fracture toughness parameter, Q_C, which was derived using a strain failure criterion for fibers in the load-carrying ply. Sun and Vaiday [11] also proposed a single fracture parameter, stress intensity factor in the load-carrying ply which was derived using classical lamination theory and LEFM theory.

In this chapter, exact LEFM analytical expression for lay-up independent failure model is presented and it is compared with the similar methodology proposed by Sun and Vaiday [11]

2.2 Stress Intensity Factor Measurements

2.2.1 Experimental Background

As mentioned earlier we have analyzed the results of fracture tests performed by Sun et al. [11, 12]. The material properties, laminate configurations used and failure load are presented here for the sake of completion. Nine different laminate configurations made from AS4/3501-6 (Hercules) graphite/epoxy were tested. The panels were made of unidirectional prepreg tape with a nominal thickness of 0.127 mm. The material properties for this unidirectional prepreg tape are shown in Table 2-1. The panel specifications, geometry, and coordinate system used for the present analysis is shown in Figure 2-1. All the test specimens reported here were fabricated using the hand lay-up technique and cured in an autoclave. Different laminate configurations were selected such that each one had at least one principal load-carrying ply (0E), i.e., plies with fibers aligned along the loading direction.

Table 2-1 Material properties of unidirectional AS4/3501-6 graphite/epoxy

Material	Young's Moduli (GPa)		Poisson's Ratio	Shear modulus	Prepreg thickness
	E_L	E_T	ν_{LT}	G_{LT}, (GPa)	(mm)
graphite/epoxy	138	9.65	0.3	5.24	0.127

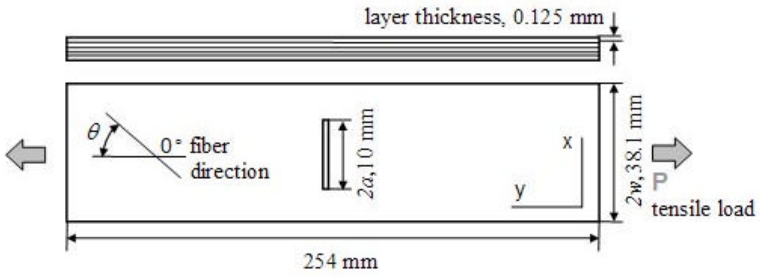

Figure 2-1 Specimen specification and fiber directions

To make the crack, a starter hole was first drilled in the laminates to minimize any delamination caused by the waterjet. The crack was then made by a waterjet cut and further extended with a 0.2 mm thick jeweler's saw blade.

The failure stress (load over nominal cross section of the laminate) for each laminate configuration tested are shown in Table 2-2. The fracture toughness estimated using the nominal stress intensity factor for the laminate is shown under the column "Laminate fracture toughness". This is computed using the formula

$$K_Q = s_y^{\infty} Y(a/w)\sqrt{pa} \tag{1}$$

where s_y^{∞} is the remote stress and Y is the finite-width correction factor. Sun et al. [11, 12] used the Y for isotropic material which is equal to 1.0414 for the present case (a/w=0.2627). One can note that the fracture toughness estimated using this method is not the same for different laminates and hence cannot be considered as a material property. The last column of Table 2-2 is the fracture toughness of the load-carrying ply calculated by Sun and Vaiday [11], which will be discussed in subsequent sections.

Table 2-2 Fracture toughness of AS4/3501-6 graphite epoxy laminates [11]

Notation	Laminate configuration	Failure stress (MPa)	Laminate fracture toughness K_Q $\left(MPa\sqrt{m}\right)$	Fracture toughness of the load-carrying ply K_Q^L $\left(MPa\sqrt{m}\right)$
S1	$[0/90/\pm45]_s$	343.00	44.83 ± 3.05	115.66
S2	$[\pm45/90/0]_s$	323.27	42.19 ± 1.87	108.82
S3	$[90/0/\pm45]_s$	316.05	41.25 ± 1.46	106.43
S4	$[0/\pm15]_s$	695.84	90.82 ± 4.01	101.81
S5	$[0/\pm30]_s$	466.14	60.84 ± 3.14	101.00
S6	$[0/\pm45]_s$	351.14	45.83 ± 2.17	106.32
S7	$[0/90]_{2s}$	446.76	58.31 ± 5.30	109.04
S8	$[\pm45/0/\pm45]_s$	287.16	37.48 ± 0.43	119.81
S9	$[\pm45_2/0/\pm45]_s$	248.40	32.42 ± 0.60	123.64

2.2.2 Stress Intensity Factor Calculations

A parameter commonly used to represent the notch sensitivity of materials is the critical stress intensity factor (S.I.F.) or the fracture toughness, K_Q. Numerous investigations have attempted to determine the critical stress intensity factor for a variety of composite laminates, and those results indicate that it depends primarily on the material, laminate configuration, stacking sequence, specimen geometry and dimensions, notch length, etc. In addition, stress intensity factor is strongly affected by the extent of damage and failure modes at the notch tip. Therefore, it is a critical parameter to design composite laminates structure.

The stress intensity factor of notched laminates can be calculated in three different ways.

1. From Eq. (1) using failure stress directly from the experiment

2. Finite Element Analysis I : From the normal stress distribution obtained from a series of finite element models using the following equation.

$$K_I = \lim_{r \to 0} s_y(r,0)\sqrt{2pr} \tag{2}$$

where r is the distance from the crack tip and normal stress component $s_y(r,0)$ is the average stress of the each ply.

3. Finite Element Analysis II : From the J-integral calculated from finite element models. The relation of the energy release rate and stress intensity factor is given by the following equation [17].

$$G_I = K_I^2 \left(\frac{a_{11}a_{22}}{2} \right)^{1/2} \left[\left(\frac{a_{22}}{a_{11}} \right)^{1/2} + \frac{2a_{12} + a_{66}}{2a_{11}} \right]^{1/2} \tag{3}$$

where a_{ij} are elastic constants. When the remote applied stress is the failure stress, stress intensity factor K_I becomes the fracture toughness K_Q. The stress intensity factor of the load-carrying ply, K_Q^L, can be estimated in two different ways.

1. From simple stress analysis using LEFM and lamination theory by calculating the portion of the applied load that is carried by the load-carrying ply. The analytical derivation of the fracture toughness of the load-carrying ply is presented in following section.

2. Same procedure as in Eq. (2) but using normal stress field of the load-carrying ply extracted from a series of finite element models using the following equation.

$$K_I^L = \lim_{r \to 0} s_y^L(r,0)\sqrt{2pr} \tag{4}$$

In order to estimate fracture toughness of various laminates configurations, the failure stresses of the notched laminates have to be determined from experiments. However, if the general fracture parameter, the fracture toughness of the load-carrying ply which is lay-up independent, is determined from preliminary test, laminates fracture toughness can be obtained using simple analysis. Consequently, it will be discussed in the following section.

2.3 Derivation of Stress Intensity Factor in the Load-Carrying Ply

In this section, we derive an analytical expression for the stress intensity factor for the load-carrying ply in terms of the average laminate stress intensity factor obtained using three methods mentioned earlier. The derivation of stress intensity factor presented here is based on LEFM and classical lamination theory. The detailed derivation procedure can be found in Appendix A and B.

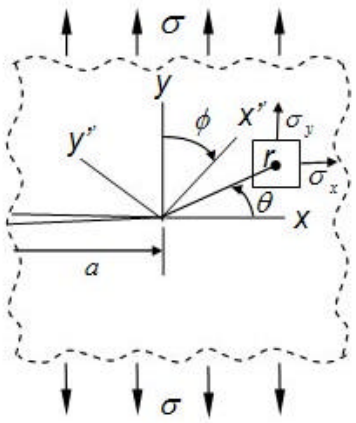

Figure 2-2 Local coordinate system of crack tip area stress components

The state of stress in the vicinity of a crack in an orthotropic material is given by

$$s_y(r,0) = \frac{K_I}{\sqrt{2pr}}\mathrm{Re}[1] \tag{5.a}$$

$$s_x(r,0) = \frac{K_I}{\sqrt{2pr}}\mathrm{Re}[-s_1 s_2] \tag{5.b}$$

where the parameters s_1 and s_2 are related to the orthotropic elastic constants as explained in Appendix B. We will use a new laminate parameter b to denote the ratio between the two normal stresses shown in Eqs. (5.a) and (5.b).

$$b = \frac{s_x(r,0)}{s_y(r,0)} = \mathrm{Re}[-s_1 s_2] \tag{6}$$

We will use the classical lamination theory to extract the stresses in the load-carrying ply from the force resultants acting in the entire laminate. According to the classical lamination theory presented in Appendix A, in the case of symmetric laminated plates without coupling under plane stress or plane strain conditions, the force-mid-plane strain equations can be expressed in matrix form as

$$\begin{Bmatrix} N_x \\ N_y \\ N_{zy} \end{Bmatrix} = \begin{bmatrix} A_{11} & A_{12} & A_{16} \\ A_{12} & A_{22} & A_{26} \\ A_{16} & A_{26} & A_{66} \end{bmatrix} \begin{Bmatrix} e_x^0 \\ e_y^0 \\ g_{xy}^0 \end{Bmatrix} \tag{7}$$

where $[A]$ is the laminate extensional stiffness matrix. The inverse relation is given by

$$\begin{Bmatrix} e_x^0 \\ e_y^0 \\ g_{xy}^0 \end{Bmatrix} = \begin{bmatrix} A_{11}^* & A_{12}^* & A_{16}^* \\ A_{12}^* & A_{22}^* & A_{26}^* \\ A_{16}^* & A_{26}^* & A_{66}^* \end{bmatrix} \begin{Bmatrix} N_x \\ N_y \\ N_{xy} \end{Bmatrix} \tag{8}$$

where superscript * denotes the component of inverse matrix of $[A]$. The stresses in the load-carrying ply can be derived from the mid-plane strains as

$$\begin{Bmatrix} s_x^L \\ s_y^L \\ t_{xy}^L \end{Bmatrix} = \begin{bmatrix} \overline{Q}_{11}^L & \overline{Q}_{12}^L & \overline{Q}_{16}^L \\ \overline{Q}_{12}^L & \overline{Q}_{22}^L & \overline{Q}_{26}^L \\ \overline{Q}_{16}^L & \overline{Q}_{26}^L & \overline{Q}_{66}^L \end{bmatrix} \begin{Bmatrix} e_x^0 \\ e_y^0 \\ g_{xy}^0 \end{Bmatrix} \tag{9}$$

where superscript ^{L} indicates the load carrying ply and the quantities Q_{ij} (i,j = 1, 2, 6) are the stiffness coefficients of the principal load carrying plies. Substituting Eq. (8) into Eq. (9) yields the following equation.

$$\begin{Bmatrix} s_x^L \\ s_y^L \\ t_{xy}^L \end{Bmatrix} = \begin{bmatrix} \overline{Q}_{11}^L & \overline{Q}_{12}^L & \overline{Q}_{16}^L \\ \overline{Q}_{12}^L & \overline{Q}_{22}^L & \overline{Q}_{26}^L \\ \overline{Q}_{16}^L & \overline{Q}_{26}^L & \overline{Q}_{66}^L \end{bmatrix} \begin{bmatrix} A_{11}^* & A_{12}^* & A_{16}^* \\ A_{12}^* & A_{22}^* & A_{26}^* \\ A_{16}^* & A_{26}^* & A_{66}^* \end{bmatrix} \begin{Bmatrix} N_x \\ N_y \\ N_{xy} \end{Bmatrix} \tag{10}$$

In the vicinity of the crack tip the force resultants can be written in terms of the average stresses in the orthotropic laminate

$$N_x = t s_x = tb s_y, \; N_y = t s_y, \; N_{xy} = t t_{xy} = 0 \tag{11}$$

where t is the total thickness of laminates. Substituting from Eq. (11) into Eq. (10) we obtain the stresses in the load-carrying ply as

$$\begin{Bmatrix} \sigma_x^L \\ \sigma_y^L \\ \tau_{xy}^L \end{Bmatrix} = \begin{bmatrix} \bar{Q}_{11}^L & \bar{Q}_{12}^L & \bar{Q}_{16}^L \\ \bar{Q}_{12}^L & \bar{Q}_{22}^L & \bar{Q}_{26}^L \\ \bar{Q}_{16}^L & \bar{Q}_{26}^L & \bar{Q}_{66}^L \end{bmatrix} \begin{Bmatrix} A_{11}^* \beta + A_{12}^* \\ A_{12}^* \beta + A_{22}^* \\ A_{16}^* \beta + A_{26}^* \end{Bmatrix} (t\sigma_y) \tag{12}$$

In particular we are interested in the stress component σ_y^L responsible for fracture and it is obtained from Eq. (9) as

$$\sigma_y^L = \left[\bar{Q}_{12}^L \left(A_{11}^* \beta + A_{12}^*\right) + \bar{Q}_{22}^L \left(A_{12}^* \beta + A_{22}^*\right)\right] (t\sigma_y) \tag{13}$$

Then the stress intensity factor K_Q^L in the load-carrying ply can be expressed in terms of the laminate stress intensity factor K_Q as

$$K_{Q(A)}^L = t \left[\bar{Q}_{12}^L \left(A_{11}^* \beta + A_{12}^*\right) + \bar{Q}_{22}^L \left(A_{12}^* \beta + A_{22}^*\right)\right] K_Q \tag{14}$$

In deriving Eq. (14) we have used the assumption $\sigma_y^L / \sigma_y = K_Q^L / K_Q$.

The lay-up independent fracture criteria assume that there is a critical value of K_Q^L for each material system and is independent of laminate configuration as long as there is a load-carrying ply in the laminate. In order to verify this concept we computed K_Q from the experimental failure loads [11] using Eq. (1). Then K_Q^L at the instant of fracture initiation was computed using Eq. (14). The resulting fracture toughness will be called $K_{Q(A)}^L$.

Sun and Vaiday [11] used a similar approach to calculate the stress intensity factor in the load-carrying ply, but they used the remote stresses applied to the laminate

in order to determine the ratio of s_x / s_y. Since the applied load is uniaxial, this ratio was equal to zero in their case. This is equivalent to taking the factor b as equal to zero. It should be emphasized that this stress ratio is not equal to zero in the vicinity of the crack tip, as there is a nonzero component of s_x is present (see Eq. 5b). We denote this fracture toughness as $K^L_{Q(B)}$. Thus the relation between $K^L_{Q(B)}$ and K_Q can be obtained by setting b =0 in Eq. (14) and it takes the form

$$K^L_{Q(B)} = t \left[\overline{Q}^L_{12} A^*_{12} + \overline{Q}^L_{22} A^*_{22} \right] K_Q \qquad (15)$$

2.4 Results and Discussion

The values of $K^L_{Q(A)}$ and $K^L_{Q(B)}$ are shown in Figure 2-3 for the nine laminate configurations. The average values and corresponding standard deviation are 74.35 MPa-$m^{1/2}$ and 18.35 % for $K^L_{Q(A)}$, and 110.28 MPa-$m^{1/2}$ and 9.8 % for $K^L_{Q(B)}$. Surprisingly the case *B* wherein the b value was taken as zero yielded consistent layer independent fracture toughness compared to the case *A* where the actual stress ratio (b>0) was used.

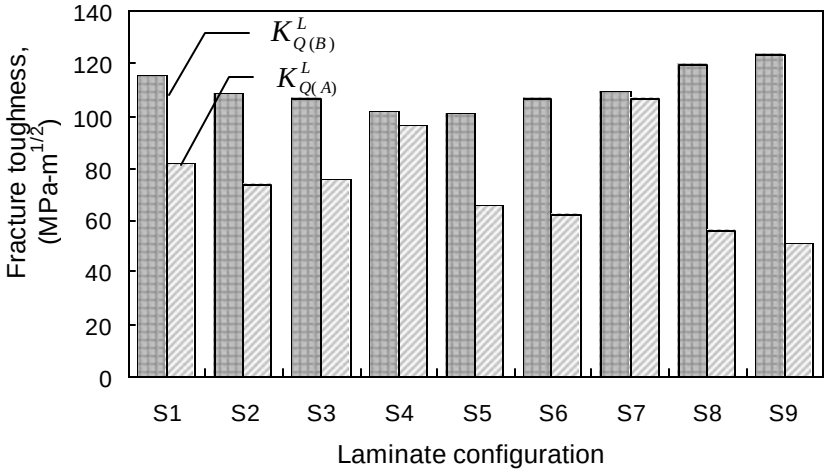

Figure 2-3 Comparison of the fracture toughness of the load-carrying ply

Such analyses are approximate, since they do not consider any stress redistribution caused by physical fracture behavior such as local damage in the form of matrix cracking, delamination, etc. In order to fully understand the nature of crack tip stress field in finite-width laminates a detailed finite element analysis was performed. The procedures and the results are discussed in Chapter 3.

CHAPTER 3
FINITE ELEMENT ANALYSIS

A detailed finite element analysis of fracture behavior of notched laminated composites was conducted in conjunction with the analytical failure models described earlier. The purpose of the finite element analysis was to develop a model that could predict the fracture parameters of notched laminated composites and investigate the effect of local damage and crack tip shape on the stress intensity factor for notched laminated composites. Another goal of the study was to determine the orthotropic finite-width correction factor using *J*-integral. One of the leading commercial FE packages, ABAQUS 6.2 [18] was used to analyze the various test specimens. Two types of analyses were performed. In the 2D model the specimens were modeled as orthotropic laminate. In the second model 3D solid elements were used to model the individual layers of the laminate. In both cases sub-modeling was performed to improve the accuracy of the calculated crack tip parameters such as stress intensity factor and *J*-Integral. The mode I stress intensity factor, K_I, can be calculated in two different ways based on the finite element analysis as mentioned earlier.

However, stress intensity factor of the load-carrying ply can be calculated only one way using the Eq. (4) because ABAQUS can not calculate *J*-integral for each ply level. $s_y^L(r,0)$ is extracted from normal stress field in the load-carrying ply of FE model.

The stress intensity factors obtained using the above methods from two types of FE models are compared with the analytical models in the subsequent section.

It is noted that overall analysis procedure and detailed results are presented for case of the $[0/\pm45]_s$ laminate and the results of other eight laminate configurations are summarized.

3.1 2D Finite Element Global Model

The purpose of the 2D analysis is to compare the results with the analytical model so that the effect of finite-width of the specimen can be understood. Further FE models can be used to understand the effects of blunt crack tip and also other forms of damage such as delamination and fiber splitting. The various laminate configurations with center notch were modeled with eight node plane stress elements (CPS8R element). A quarter model was used, with symmetric boundary conditions. The width of the model, *w*, was 19.05 mm, and the length was 254 mm. The notch was modeled as a sharp crack with a half width, a= 5 mm. Since the lay-up is symmetric, it was only necessary to model half of the thickness.

The main difference between global model and sub-model is mesh refinement. The FE global model uses relatively coarse mesh compared to the FE sub models. A fixed element size with width of 1 mm was used in the FE global model. A relatively fine mesh was used adjacent to the notch. The geometry and the finite element models were created using ABAQUS/CAE modeling tool and ABAQUS keyword editor. Figure 3-2 shows the initial mesh of the upper left quadrant. Separate elements were used to represent each ply and common nodes were used for interface of plies. Figure 3-1 shows the scheme of two-dimensional FE model of $[0/\pm45]_s$ laminate. Figure 3-3 shows the overall global modeling procedure in case of $[0/\pm45]_s$ laminate. The material property of each ply was modeled as a homogeneous linear elastic orthotropic material throughout

this FE analysis. In order to use a single global coordinate system, the material properties of angle plies were transformed using the transformation relation for engineering constants. Orthotropic properties for AS4/3501-6 graphite/epoxy unidirectional prepreg were defined as shown in Table 2-1. The material property of each angle ply was implemented in ABAQUS by means of user material subroutine (UMAT). The fixed grip loading condition was simulated by constraining the nodes along the edge of the plate to have the same displacement under an applied load. This was also implemented by using the EQUATION command. The failure load obtained from experiments (see Table 2-1) was applied. In global model analysis, *J*-integral also was calculated using ten contour lines to determine the orthotropic finite-width correction factors. It will be discussed in Chapter 3.4.

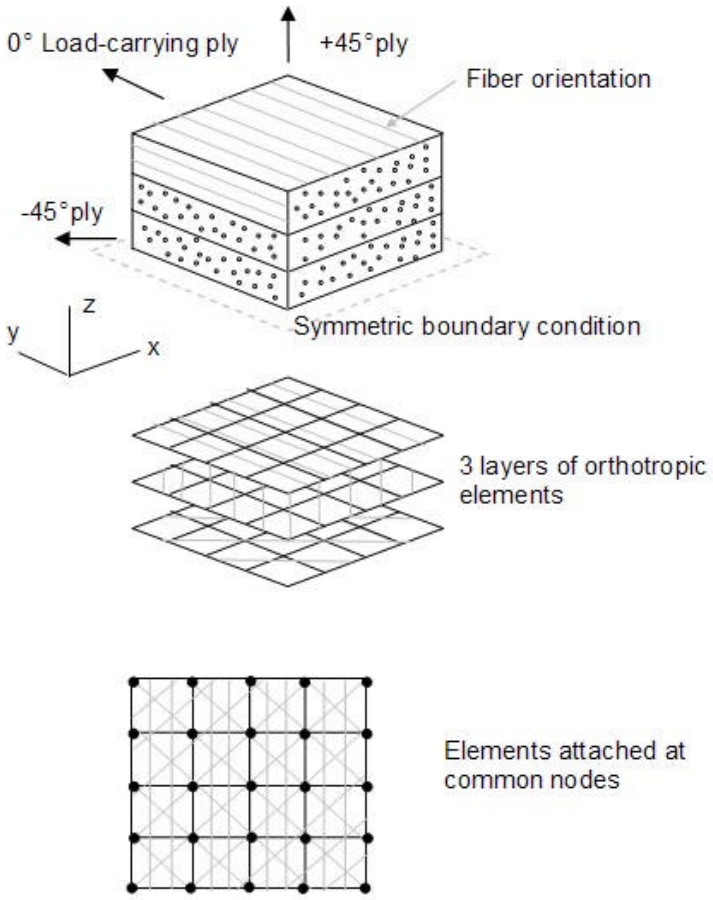

Figure 3-1 Scheme of two-dimensional FE model of $[0/\pm45]_s$ laminate

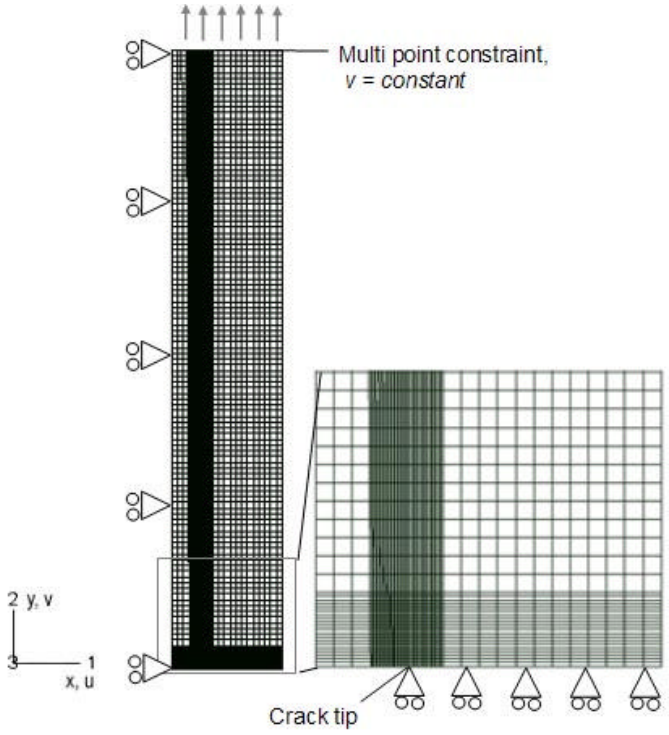

Figure 3-2 Finite element global model mesh and boundary condition

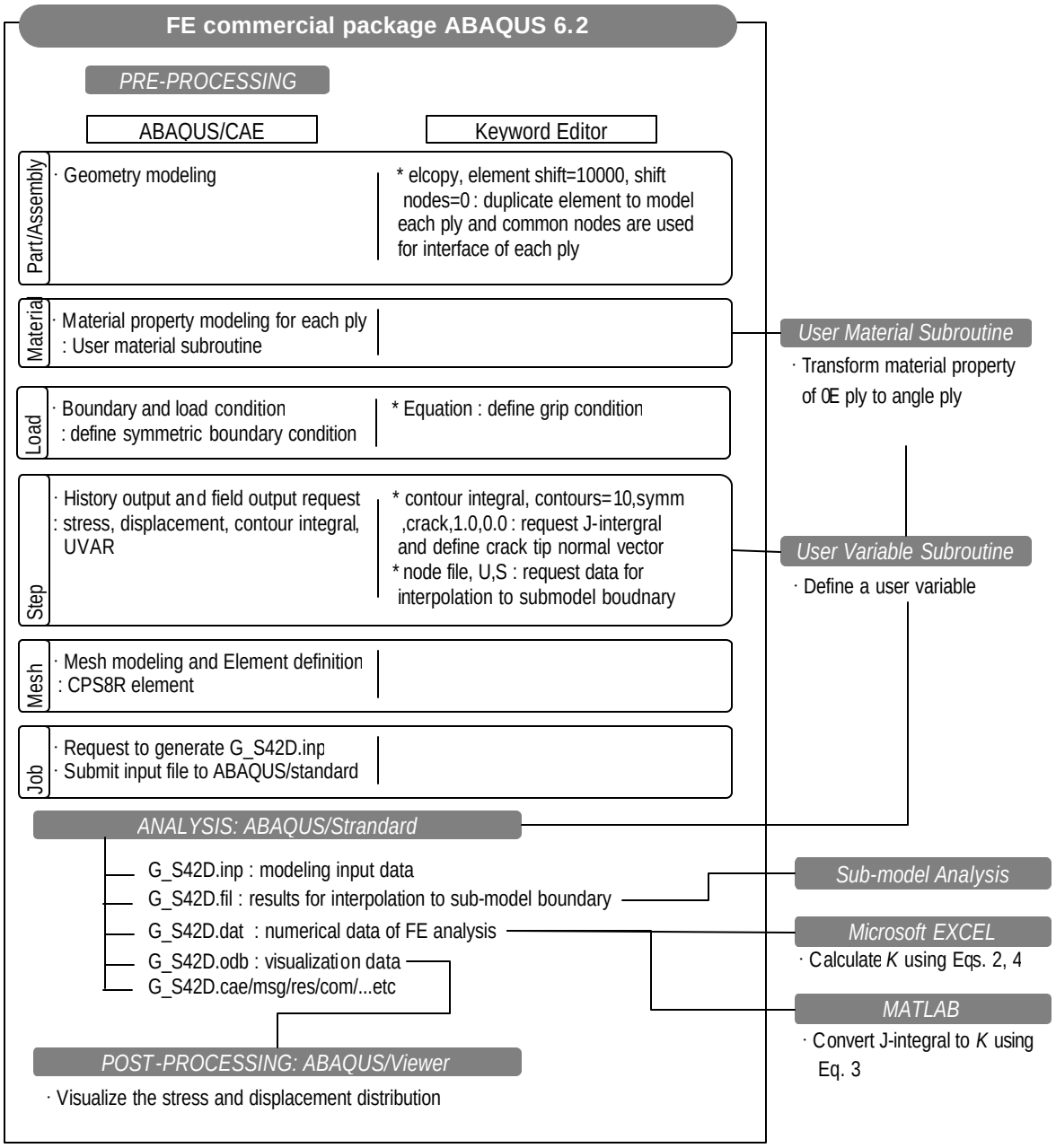

Figure 3-3 Scheme of 2D FE global model analysis procedure

Figure 3-4 shows the distribution of normal stress of the load-carrying ply and average normal stress of the laminate, respectively, for the global model. From the normal stress distribution in the Figure 3-4, it is clear that s_y stress in the load-carrying ply is much higher than the average and hence that of angle ply. In the Figure, $\bar{s}_y$ was defined as $\frac{s_y^L + s_y^{+45} + s_y^{-45}}{3}$. A contour plot of s_y distribution is shown in Figure 3-6. Figure 3-5 shows the values of $s_y^L\sqrt{2pr}$ and $\bar{s}_y\sqrt{2pr}$ as a function of r in the $[0/\pm45]_s$ laminate. The stress intensity factor of the load-carrying ply and the laminate can be obtained by extrapolating measured normal stress distribution from the FE global model based on Eqs. (2) and (4). The stress intensity factor obtained from global FE model agree well with the analytical model case B (Eq. 15) which was calculated assuming s_x = 0 ahead of crack tip.

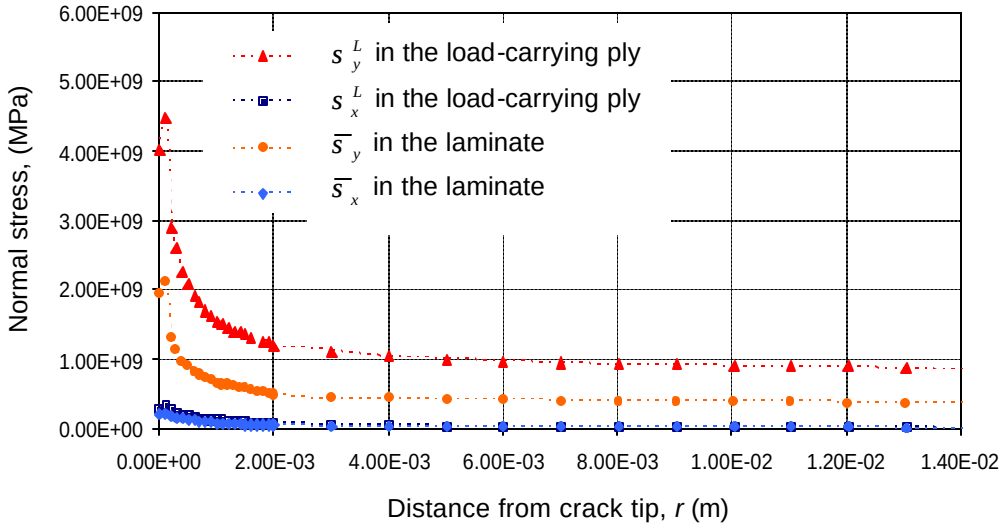

Figure 3-4 Normal stress distribution in the global model in the $[0/\pm45]_s$ laminate

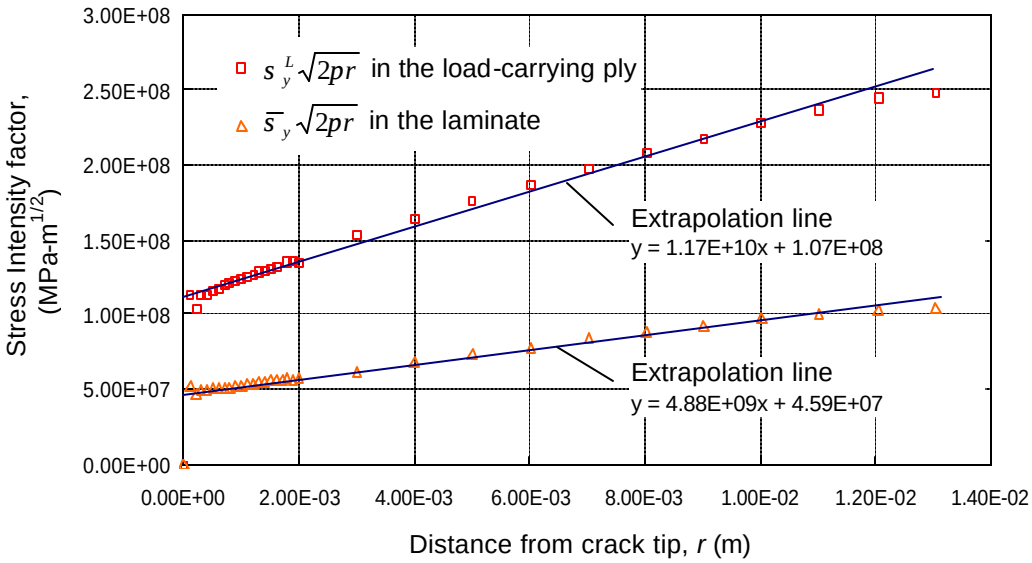

Figure 3-5 Stress intensity factor in the global model for $[0/\pm45]_s$ laminate

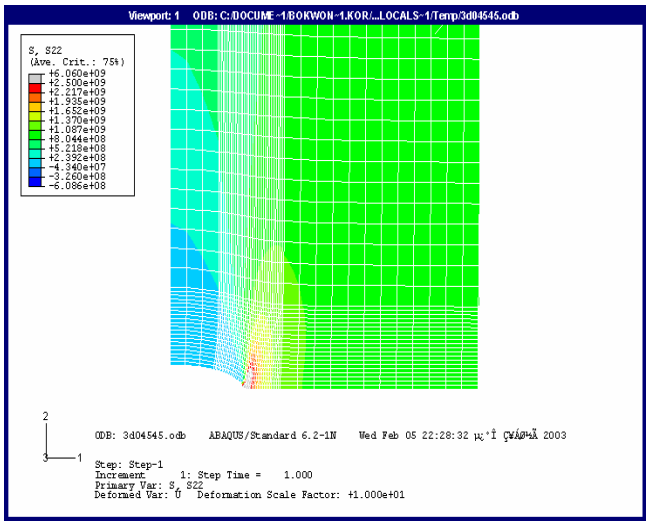

(a) Load-carrying ply, 0Edegree

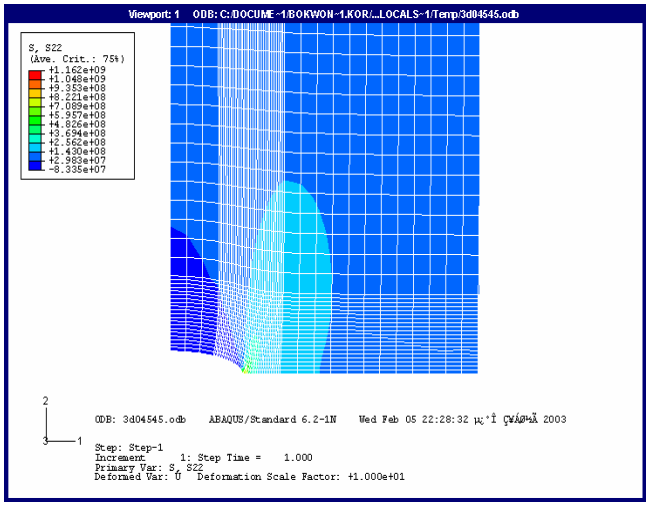

(b) +45E ply

Figure 3-6 s_y distribution in the $[0/\pm45]_s$ laminate under a load of 351.14 MPa

3.2 2D Finite Element Sub-Model

The analysis was repeated with a very refined element size in order to investigate the local fracture behavior and the sensitivity of the results to mesh refinement. All other aspects of the analysis were kept the same as global model. For efficiency of computation, the finite element sub-modeling analysis technique was adopted. The sub-modeling analysis is most useful when it is necessary to obtain an accurate, detailed solution in a local area region based on interpolation of the solution from an initial, relatively coarse, global model. The sub-model is run as a separate analysis. The link between the sub-model and the global model is the transfer of results saved in the global model to the relevant boundary nodes of the sub-model. Thus, the response at the boundary of the sub-model is defined by the solution of the global model. However, in order to adopt sub-modeling technique, the accuracy of sub-model should be ensured by checking the comparing important parameter to determine reasonable sub-modeling size. Three different sizes of sub-models were modeled to determine adequate sub-model size to minimize the execution time and maximize accuracy. Figure 3-7 shows the different size of sub-model and Figure 3-8 shows the results of comparison of stress intensity factor obtained from sub-models with stress intensity factor obtained from *J*-integral using Eq. (3). For efficiency of computation, sub-model size *B* was chosen for subsequent studies.

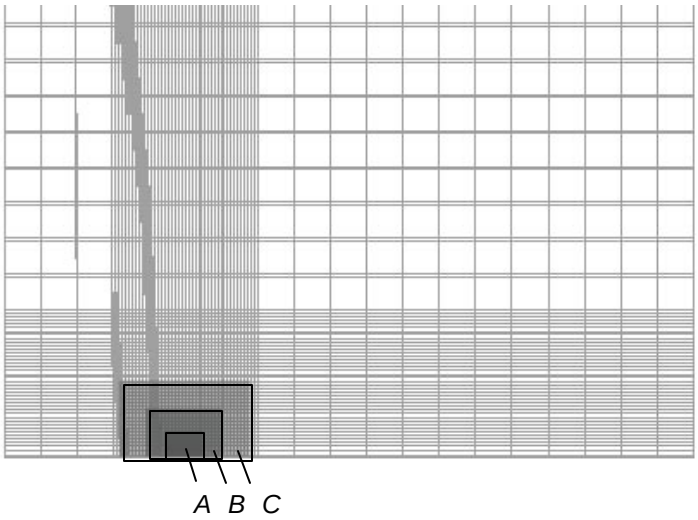

Figure 3-7 Different sizes of sub-model (*A*= 10 %, *B*= 20 %, *C*= 40 % of crack size, *a*)

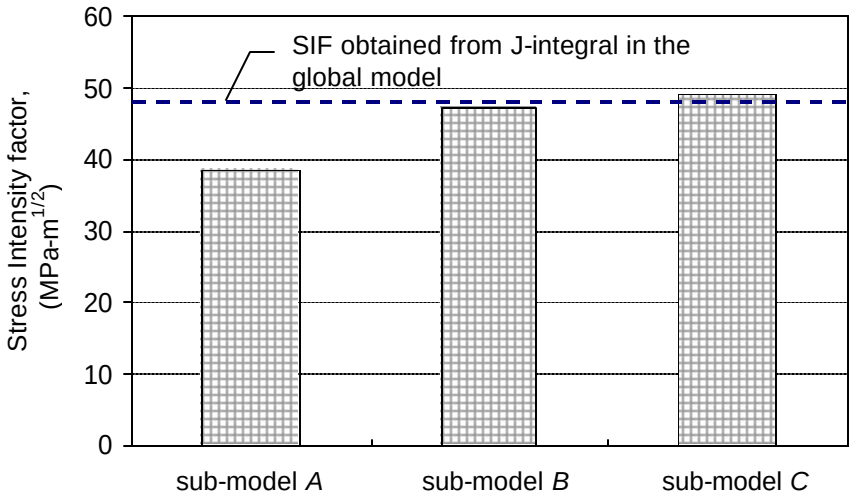

Figure 3-8 Comparison of SIF obtained from different sizes of sub-model

A fixed mesh size, 0.01 mm was used in the sub-model and overall size of sub-model is 20% of crack size, *a*. Figure 3-9 shows sub-model mesh and linking with global model.

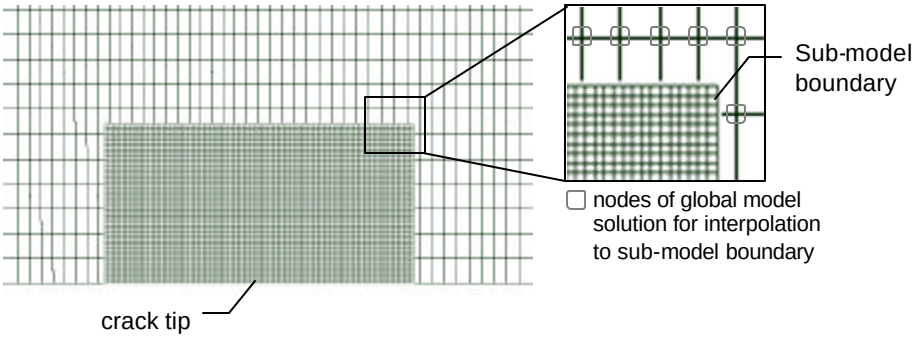

Figure 3-9 Finite element sub-model mesh and linking with global model

Figure 3-10 shows the distribution of normal stress of the load-carrying ply and average normal stress of the laminate, respectively, for the sub-model. From the Figure for normal stress distribution (Fig. 3-10), it can be seen that the nature of stress variation is similar to that of global model shown in Figure 3-4. Same procedures of global model analysis were repeated to estimate the stress intensity factor of the load-carrying ply and the average stress intensity factor for the laminate in the sub-model. It is noted that the average stress intensity factor for the laminate obtained from the sub-model, 45.7 MPa-$m^{1/2}$, is almost same as that of global model, 45.9 MPa-$m^{1/2}$. However, the stress intensity factor of the load-carrying ply, 59.2 MPa-$m^{1/2}$, is much less compared to that of global model, 107 MPa-$m^{1/2}$.

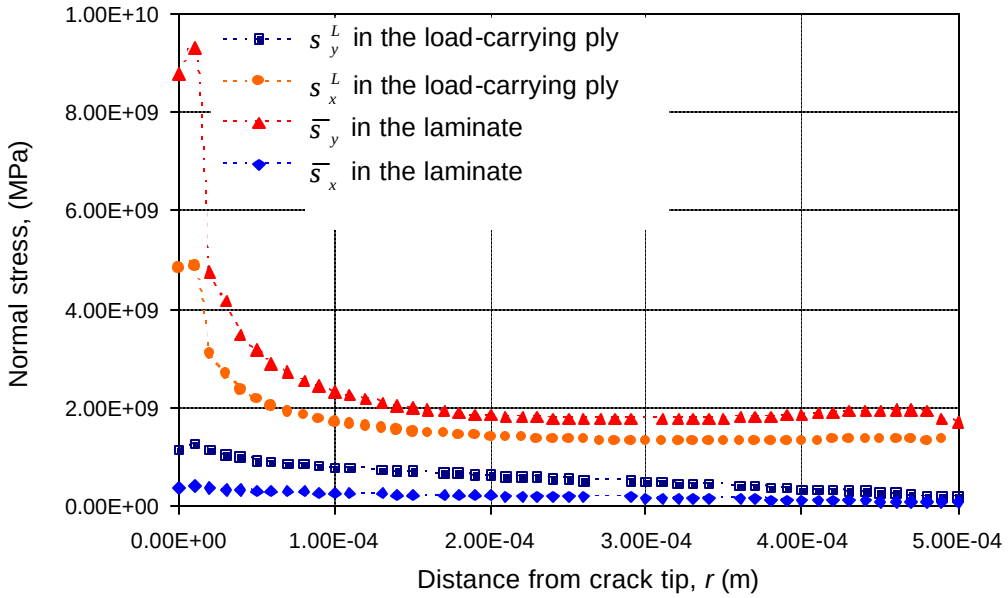

Figure 3-10 Normal stress distribution in the sub-model in case of [0/±45]s laminate

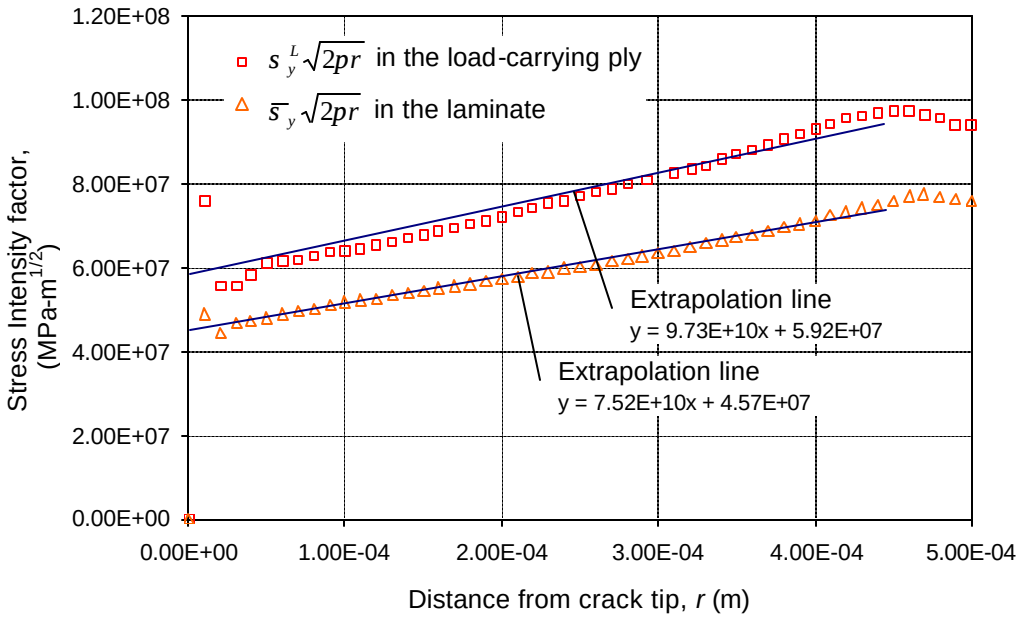

Figure 3-11 Stress intensity factor in the sub-model in case of $[0/\pm45]_s$ laminate

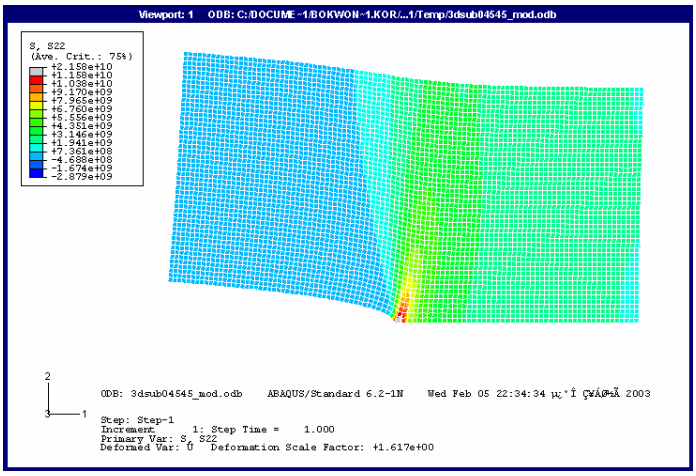

(a) Load-carrying ply, 0Edegree

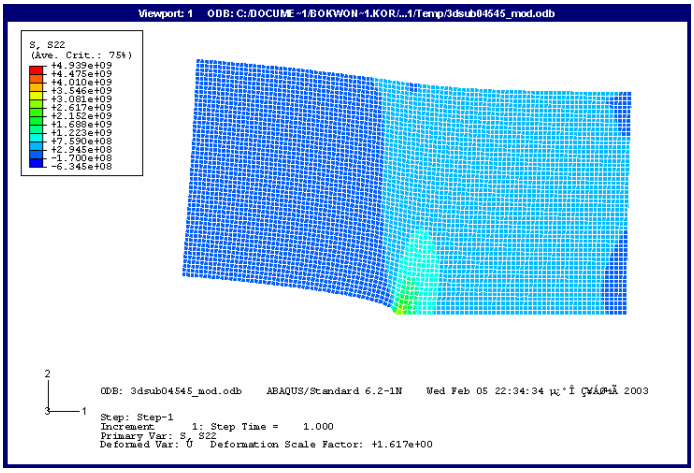

(a) +45 ply

Figure 3-12 s_y distribution in the $[0/\pm45]_s$ laminate under a load of 351.14 MPa

3.3 Comparison of FE Results and Analytical Model

The stress intensity factor in the load-carrying ply was calculated using both the global and sub-model. The laminate stress intensity factors calculated from the two models were in good agreement for all laminate configurations indicating that the mesh refinement was sufficient. From the laminate stress intensity factor, we can calculate the finite-width correction factor Y using the relation

$$K_Q = s_y^{\infty} Y \sqrt{pa} \tag{16}$$

The values of Y for various laminate configurations are shown as a function of a/w and b in Figure 3-21. It has been found that the finite-width correction factor is a strong function of the newly introduced lamination parameter b. More on this effect and significance of b will be presented in Chapter 3.4. The results for the load-carrying ply stress intensity factor yielded some interesting trends. The results of K_Q^L estimated through the finite element analysis are shown in Figure 3-16 and compared with two analytical models. The $K_{Q(B)}^L$ calculated from Eq. (15) agrees well with the results of the global model, which has a relatively coarse mesh. On the other hand, the $K_{Q(A)}^L$ calculated from the exact LEFM solution, Eq. (14), shows good agreement with the results of sub-model, which has a very fine mesh. It is obvious from the results that the s_x stresses ahead of the crack tip play a significant role in the estimation of K_Q^L. The coarse mesh of global model does not have sufficient nodes to capture the s_x effect, although it is good enough for determining s_y. The global model is not able to present a complete picture of stresses in the vicinity of the crack tip.

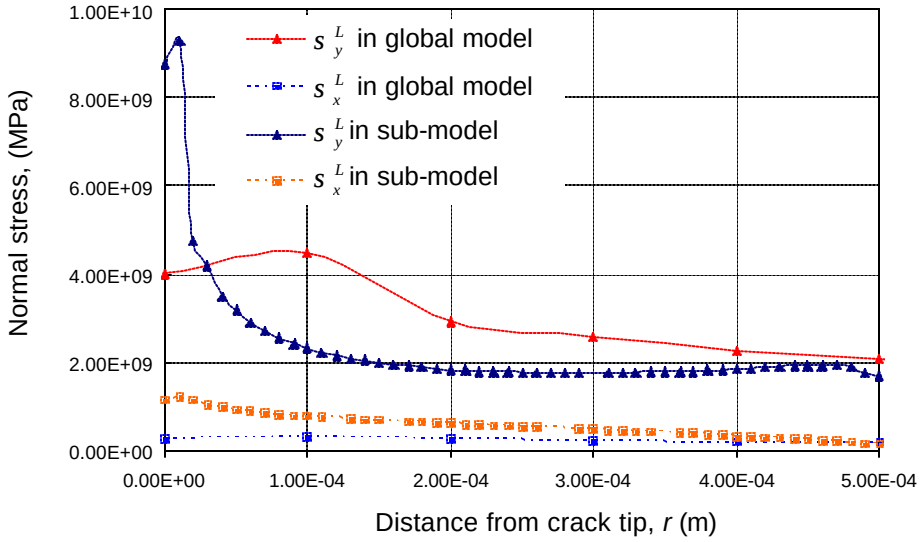

Figure 3-13 Comparison of normal stress distribution in the sub-model and global model in case of $[0/\pm45]_s$ laminate

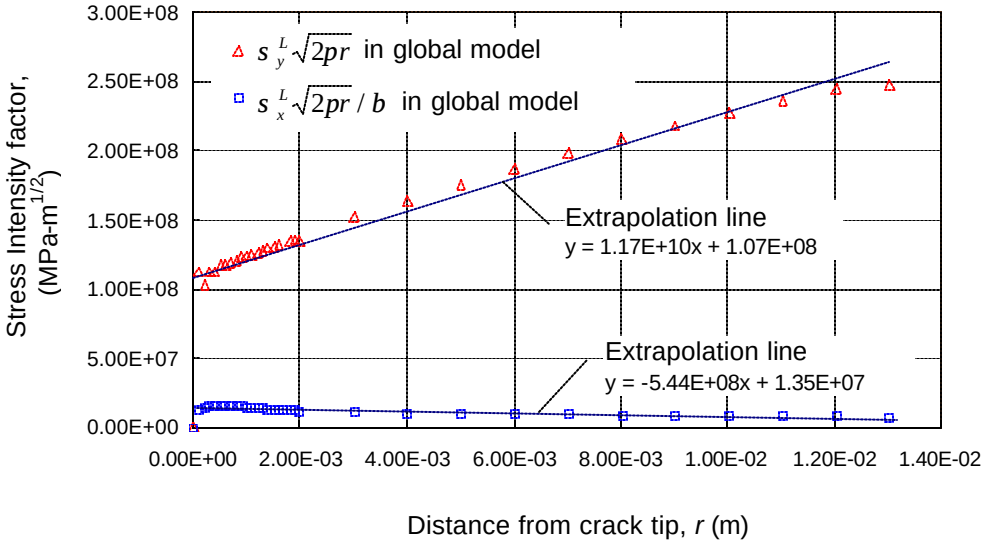

Figure 3-14 Stress intensity factor in the global model in case of $[0/\pm45]_s$ laminate

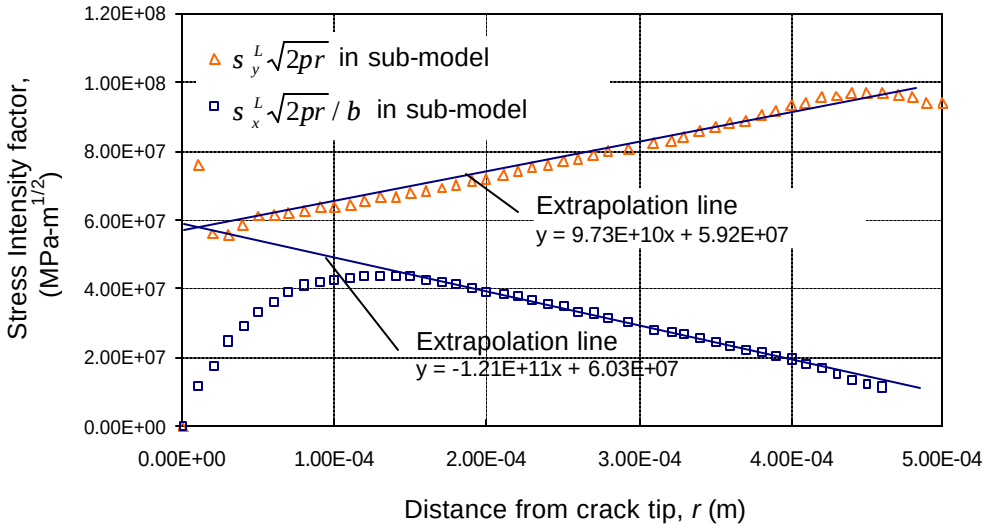

Figure 3-15 Stress intensity factor in the sub-model in case of $[0/\pm45]_s$ laminate

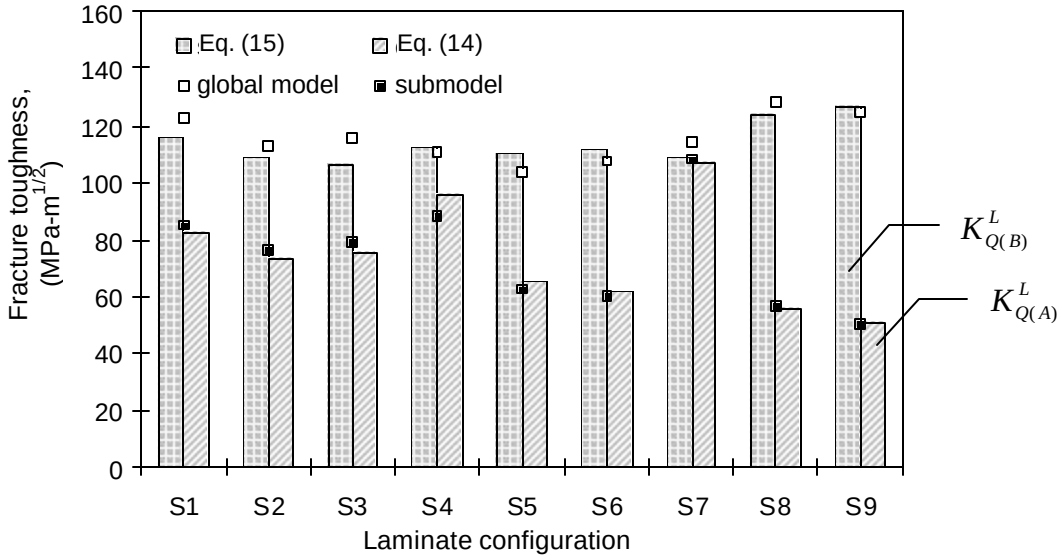

Figure 3-16 Comparisons of the fracture toughness of principal load-carrying ply

3.4 Finite-Width Correction (FWC) Factor

3.4.1 Isotropic Finite-Width Correction Factor

The lay-up independent failure model presented in Ref. [11] enables the prediction of the notched strength of composite laminates. This model was formulated assuming that the plates are of infinite width, thus, the infinite width notched strength, s_N^{∞}, is predicted. However, experimental data provide notched strength data on finite width specimens, s_N. To account for finite width of the specimen, the finite-width correction (FWC) factor Y is required to estimate the stress intensity factor accurately. According to the definition, the finite-width correction factor is a scale factor, which is applied to multiply the notched infinite solution to obtain the notched finite plate result. A common method used extensively in the literature is to relate experimental notched strength, s_N, for plates of finite width to the notched strength of plates of infinite width is to simply multiply s_N by the finite-width correction factor Y, where K_I is the mode I stress intensity factor.

$$s_N^{\infty} = s_N \frac{K_I}{K_I^{\infty}} \tag{17}$$

The mode I critical stress intensity factor for isotropic plate of finite width is calculated from following equation.

$$K_Q = Y_{ISO} s_N \sqrt{pa} \tag{18}$$

Due to the lack of an analytical expression for orthotropic or anisotropic finite-width correction factors, the existing lay-up independent failure models used isotropic finite-width correction factor, Y_{ISO}, to evaluate stress intensity factor of notched composite

laminates. Usually Y_{ISO} is a 3rd order polynomial in *a/w*, which was developed empirically for the case of center cracks in isotropic panels. For example

$$Y_{ISO} = 1 + 0.1282(a/w) - 0.2881(a/w)^2 + 1.5254(a/w)^3 \quad (19)$$

can be found in Ref. [11]

However, the isotropic finite-width correction factor does not properly account for the anisotropy exhibited by different laminate configuration. In some cases, the application of the isotropic finite-width correction factors to estimate the anisotropic or orthotropic finite-width correction factors can cause significant error.

3.4.2 Orthotropic Finite-Width Correction Factor

3.4.2.1 Developing procedure for FWC solution

To improve the accuracy of notched strength predictions for finite-width notched composite laminates, orthotropic finite-width correction factor is obviously required. There are a couple of methods to determine the orthotropic finite-width correction factor [13-15]. However, no closed form solution is available. For this purpose, closed form of orthotropic finite-width correction factor is developed empirically based on the results of finite element analysis. It is found that *Y* depends on *ß* also.

The finite-width correction factor for orthotropic plate can be obtained from following equation, where $s_y^{\infty}(x,0)$ is the normal stress distribution in an infinite plate.

$$Y_{OT} = \frac{K_I}{s_y^{\infty}\sqrt{2pa}} \quad (20)$$

where s_y^{∞} is the remote uniaxial stress, and *a* is the half crack length.

However, a closed form expression for K_I does not exist. To estimate values of K_I for various laminate configurations, the commercial finite element code, ABAQUS

6.2/Standard, was used. The stress intensity factor, K_I, can be calculated in two different ways based on the finite element analysis as mentioned earlier.

The accuracy of these methods is investigated by comparison between a known closed form solution Eq. (19) for notched isotropic plate and the solution obtained from ABAQUS finite element models. In the finite element analysis, eight node, plane stress elements were used to model notched plates made from isotropic material with material property E = 100 GPa and ν = 0.25. Geometry and mesh size of the global model were used to evaluate the J-integral for the range of crack sizes given by a/w = 0.05, 0.1, 0.2, 0.2625 (specimen), 0.3, 0.4, 0.5. Ten contour lines were used to evaluate the J-integral in the finite element models. Each contour is a ring of elements completely surrounding the crack tip starting from one crack face and ending at the opposite crack face. These rings of elements are defined recursively to surround all previous contours. ABAQUS 6.2 automatically finds the elements that form each ring from the node sets given as the crack-tip or crack-front definition. Each contour provides an evaluation of the J-integral

Figure 3-17 shows the estimated finite-width correction factor determined by finite element methods and a closed form solution for an isotropic notched plate with various notch sizes. Excellent agreement between these analysis methods is noted over the whole notch size of the plate.

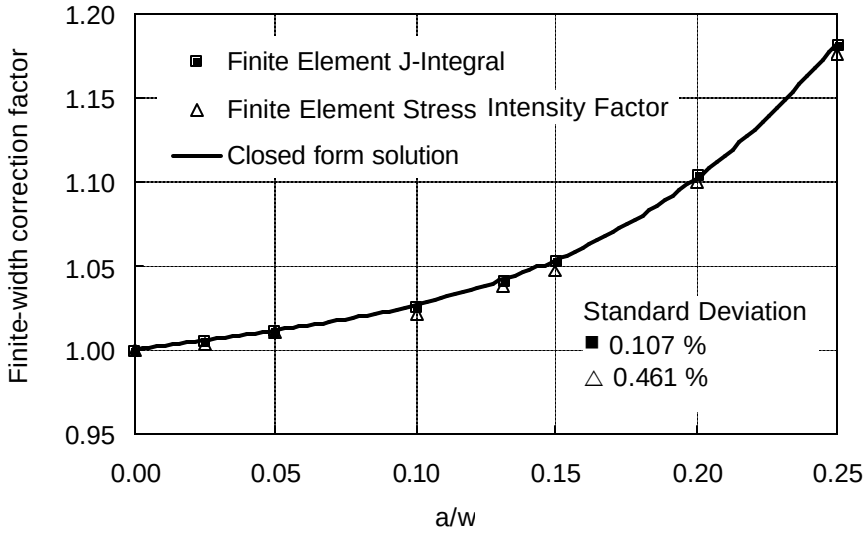

Figure 3-17 Comparison of the finite-width correction factors in an isotropic plate computed by the finite element methods with the closed form solution

The most accurate method, finite element *J*-integral, was adopted to develop the finite-width correction factor for orthotropic plates. Figure 3-18 shows the calculated *J*-integral value from FE global model for the material and lay-ups in Table 2-1. Ten contour lines were used to evaluate *J*-interagl and these values are reasonably independent of the path as expected. The first four *J*-integral values were taken to calculate average *J*-integral and it was used to estimate K_I using Eq. (3). The orthotropic finite-width correction factor obtained using Eq. (20) are shown in Figure 3-19. As expected, the finite-width correction factors increase with the crack size to panel width ratio. Additionally, the finite-width correction factor strongly depends on the anisotropy of laminate characterized by *ß*. Figure 3-20 shows the finite-width correction factor for different values of anisotropy parameter b and the b values of laminated composite panel using Eq. (6) are shown in Table 3-2.

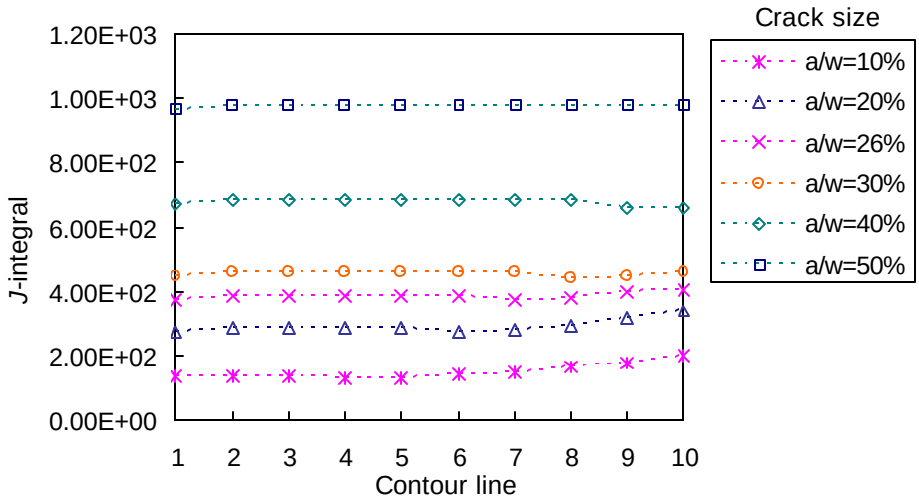

Figure 3-18 *J*-integral vs. contour line calculated from FE model of the $[0/\pm45]_s$ laminate

Table 3-1 *J*-integral value calculated from FE model of the $[0/\pm45]_s$ laminate

Crack size (a/w)	0.1	0.2	0.26	0.3	0.4	0.5
Contour 1	1.31E+02	2.72E+02	3.75E+02	4.44E+02	6.71E+02	9.63E+02
Contour 2	1.31E+02	2.81E+02	3.88E+02	4.59E+02	6.82E+02	9.75E+02
Contour 3	1.31E+02	2.81E+02	3.88E+02	4.59E+02	6.82E+02	9.75E+02
Contour 4	1.26E+02	2.81E+02	3.88E+02	4.59E+02	6.82E+02	9.75E+02
Contour 5	1.29E+02	2.81E+02	3.88E+02	4.59E+02	6.82E+02	9.75E+02
Contour 6	1.37E+02	2.70E+02	3.88E+02	4.59E+02	6.82E+02	9.75E+02
Contour 7	1.48E+02	2.76E+02	3.73E+02	4.59E+02	6.82E+02	9.75E+02
Contour 8	1.64E+02	2.87E+02	3.81E+02	4.41E+02	6.82E+02	9.75E+02
Contour 9	1.75E+02	3.16E+02	3.96E+02	4.44E+02	6.55E+02	9.75E+02
Contour 10	1.97E+02	3.38E+02	4.04E+02	4.59E+02	6.60E+02	9.75E+02

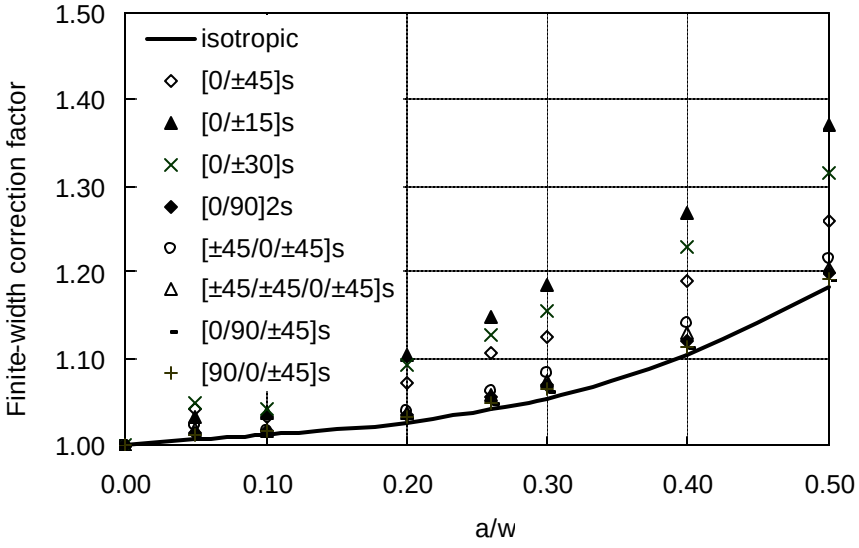

Figure 3-19 The finite-width correction factors vs. ratio of crack size to panel width

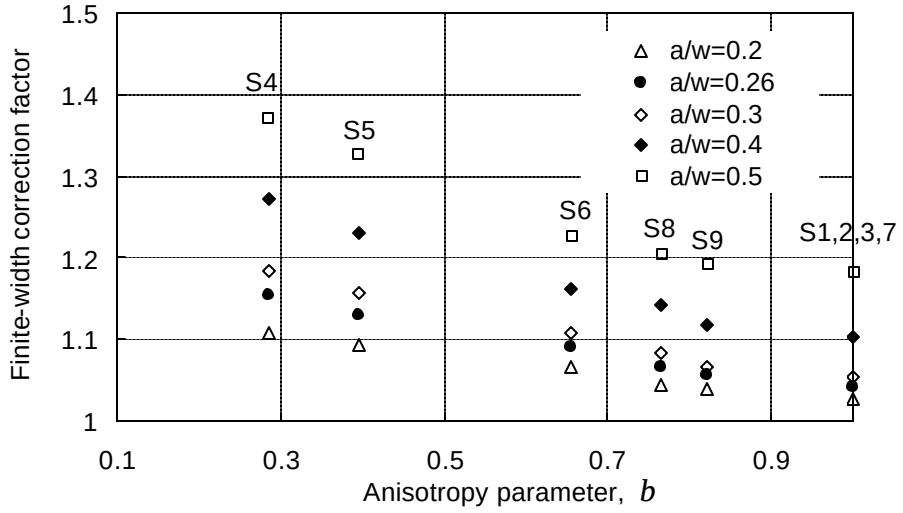

Figure 3-20 The finite-width correction factors vs. anisotropy parameter, *b*

Table 3-2 Values of the anisotropy parameter, ß, for the test specimens

specimen	S1	S2	S3	S4	S5	S6	S7	S8	S9
b	1	1	1	0.285	0.396	0.656	1	0.767	0.823

The above results indicated that there is a definite relation between the finite-width correction factors, geometric parameter, *a/w*, and anisotropy parameter, b . Thus, the general semi-empirical solution of orthotropic finite-width correction factor was developed using multiple least square regressions to fit measured data in the finite element analysis. It can be expressed in terms of ß and ratio of crack size, *a/w*, in the following form

$$Y_{OT} = 1 + b_1\left(\frac{a}{w}\right)\left(1 + c_1 B + c_2 B^2\right) + b_2\left(\frac{a}{w}\right)^2 (1 + c_3 B + c_4 B^2) + b_3\left(\frac{a}{w}\right)^3 (1 + c_5 B + c_6 B^2) \quad (21)$$

where B is defined as 1- b , and the coefficients of least square fit are shown in Table 3-3. A 3D plot of the finite-width correction factors is given in Figure 3-21 and estimated values of the factor are summarized in Table 3-4. Note that Y_{OT} increases with *a/w* and *B.*

Table 3-3 The coefficients of semi-empirical solution of orthotropic finite-width correction factor

b_1	c_1	c_2	b_2	c_3	c_4	b_3	c_5	c_6
0.1091	5.0461	-2.1324	-0.2319	-2.9103	-4.4927	1.4727	-1.5124	-0.0375

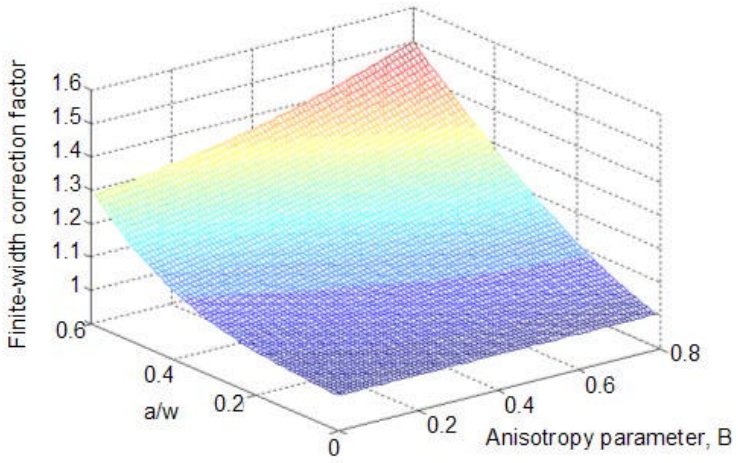

Figure 3-21 The finite-width correction factors as a function of anisotropy parameter, *ß*, and ratio of crack size to panel width, *a/w*.

Table 3-4 The finite-width correction factors obtained from the semi-empirical solution (Eq. 21)

a/w	Orthotropic, Y_{OT}									Isotropic,
	S1	S2	S3	S4	S5	S6	S7	S8	S9	Y_{ISO}
0.10	1.011	1.011	1.011	1.046	1.041	1.029	1.010	1.023	1.020	1.01
0.20	1.024	1.024	1.024	1.107	1.094	1.065	1.024	1.052	1.045	1.02
0.26	1.040	1.040	1.040	1.152	1.134	1.092	1.040	1.075	1.066	1.04
0.30	1.051	1.051	1.051	1.182	1.160	1.111	1.052	1.091	1.082	1.05
0.40	1.101	1.101	1.101	1.269	1.239	1.173	1.101	1.148	1.136	1.10
0.50	1.181	1.181	1.181	1.369	1.331	1.254	1.181	1.227	1.214	1.18

3.4.2.2 Anisotropy parameter, *ß*

The anisotropy parameter, b , has been calculated using classical lamination theory for a variety of AS4/3501-6 graphite/epoxy composite laminates. The values of b depend on both material property and laminate configuration. It is equal to 1 when the laminate is isotropic or quasi-isotropic. As the anisotropy increases, the value of b increases to certain finite value. The finite-width correction factors for orthotropic laminates depend on the ratio of crack length to panel width, *a/w*, and also the anisotropy parameter, b . In general, Y increases with *a/w* and b . A plot of variation of the anisotropy parameter as a function of q for $[\pm q]_s$ and $[0/\pm q]_s$ is given in Figure 3-22. Notice that the anisotropy parameter, b , attains a maximum value at $q = 90^o$ in $[\pm q]_s$ laminates.

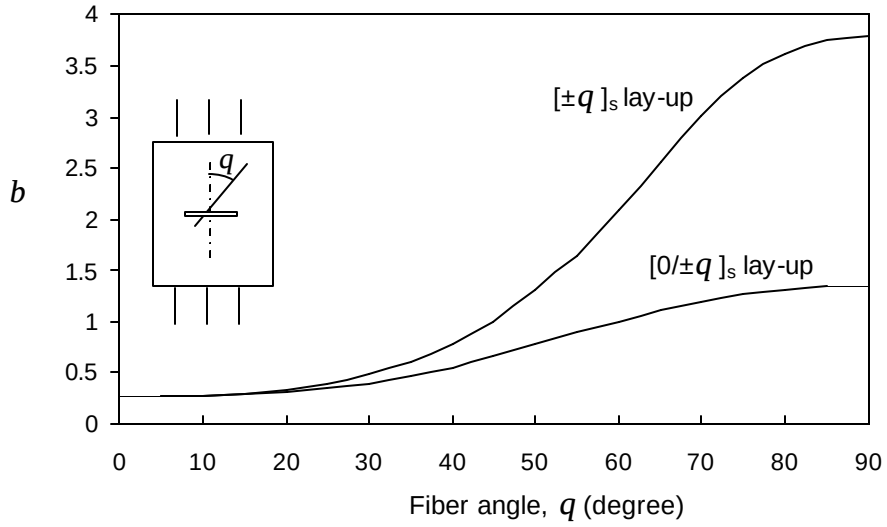

Figure 3-22 Anisotropy parameter, *ß*, as a function of lamination angle for graphite/epoxy $[\pm q]_s$ and $[0/\pm q]_s$ laminates

Anisotropy parameter, b , can be $0 \le b \le +\infty$. However, the range of the values is quite limited in most existing laminate materials. For example, the ranges of computed

values of anisotropy parameter for a few laminate materials, which are widely used in composite structures, are shown in Table 3-5.

Table 3-5 Ranges of anisotropy parameter, b , various composite materials

	Material property				Ranges of b
	E_T (GPa)	E_L (GPa)	ν_{LT}	G_{LT} (GPa)	
AS4/3501-6 graphite/epoxy	9.65	138	0.3	5.24	$0.264 \le b \le 3.781$
E-Glass/Epoxy	19.5	52	0.28	3.24	$0.612 \le b \le 1.633$
S-Glass/Epoxy	8.9	43	0.27	4.5	$0.454 \le b \le 2.198$
Kevlar 149/Epoxy	5.5	87	0.34	2.2	$0.251 \le b \le 3.977$
CFS003/LTM25 Carbon/Epoxy	54.0	54.7	0.065	4.05	$0.993 \le b \le 1.006$

The semi-empirical solution (Eq. 21) for the finite-width correction factor for an orthotropic material was developed using a curve fitting method from anisotropy parameter, $0.285 \le b \le 1$. According to the characteristic of a curve fitting method, if data for prediction is far beyond the limits of the observed data, a prediction can cause a relatively large error. However, the ranges of practical values are within small bounds. Therefore, the methodology described above can be used to develop the finite-width correction factor solution for most widely used composite materials.

3.5 Effect of Blunt Crack Tip Shape

3.5.1 2D FE Modeling Procedure

The effect of the shape of the crack tip is not considered in any of the fracture models when calculating stress intensity factor that controls the laminate failure. The effects of different initial crack tip shape were analyzed. According to the specimen preparation process [11], to make the initial cracks, a starter hole was first drilled in the laminate to minimize any delamination caused by the waterjet. The crack was made by

waterjet cut and further extended with a 0.2mm thick jeweler's saw blade. Thus, in the present analysis, the crack tip thickness was assumed less than 0.2mm and three different crack tip shapes, elliptical, triangle, and rectangular, were considered. These assumptions were carefully investigated through the series of FE sub-models and the results are discussed below for the case of $[0/\pm45]_s$ laminate.

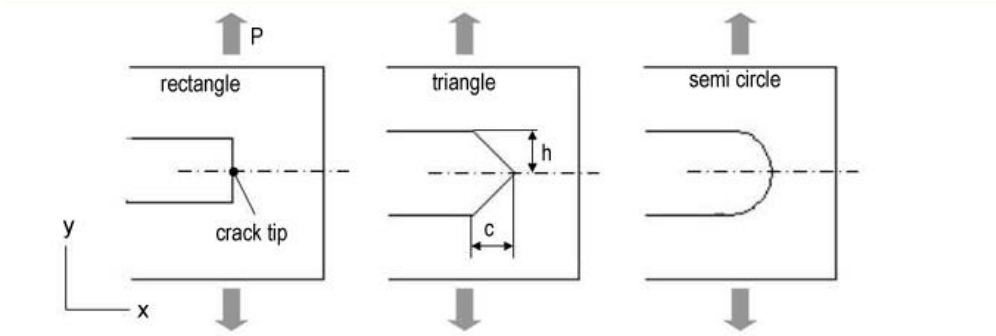

Figure 3-23 Crack tip shape profiles

3.5.2 Results and Discussion

Figures 3-24 and 3-25 compare the effect of crack tip profile and crack thickness on the stress intensity factor of principal load-carrying ply using global and sub-model. In this analysis, thickness of the crack was assumed to be less than 0.2 mm. The global nature of FE models requires that the details of the crack tip shape are not explicitly modeled due to the mesh size. Therefore, the global model may not accurately capture the details near the crack tip and is not reliable in capturing the behavior of the crack tip shape. From the results of the global model, it is evident that stress intensity factors of global model are not greatly influenced by crack tip shape.

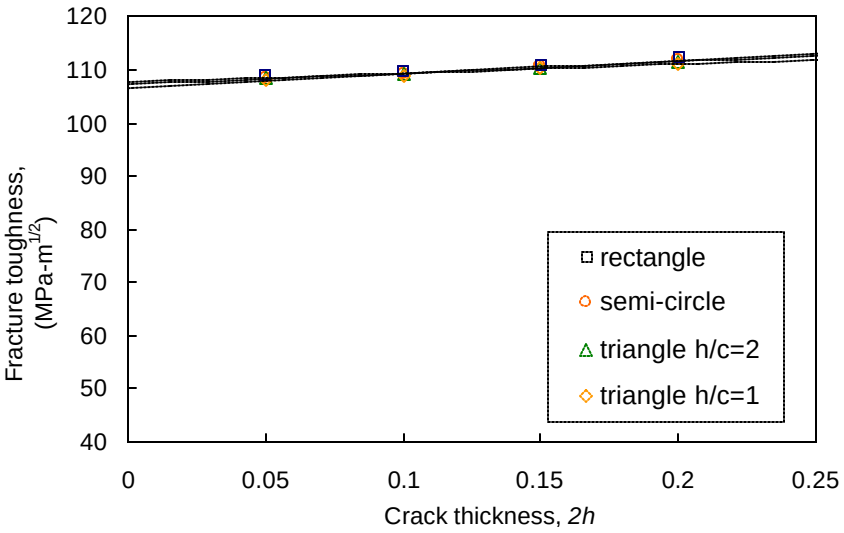

Figure 3-24 Effect of crack tip shape on predicted fracture toughness of $[0/\pm45]_s$ laminate ; 2D FE global model results

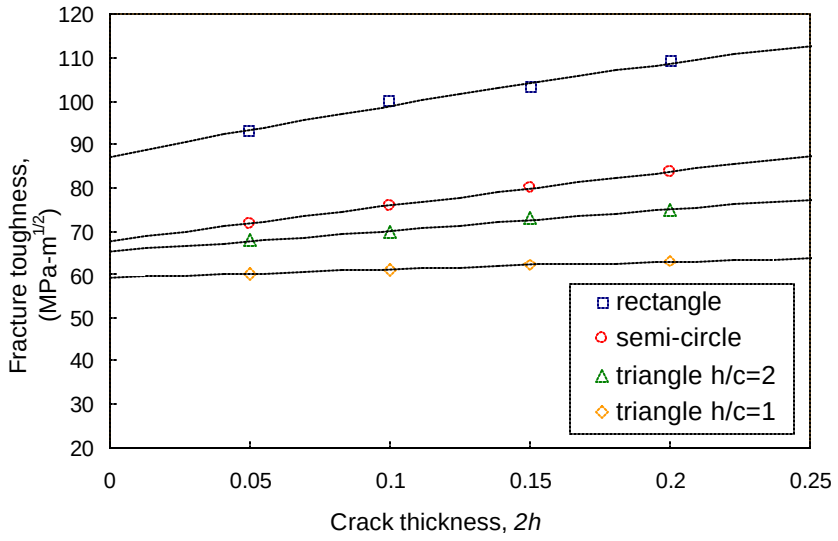

Figure 3-25 Effect of crack tip shape on predicted fracture toughness of $[0/\pm45]_s$ laminate ; 2D FE sub-model results

However, the results of the sub-model indicate that the crack tip shape has a significant effect on the stress intensity factor at the crack tip. Furthermore, the large variation was observed in the results shown in Figure 3-25. It indicates that the stress intensity factor is very sensitive to the crack tip slope ahead of the crack tip. The results shows that the crack tip slope near the crack tip is a more critical parameter than the crack tip thickness. The results clearly indicate that the stress intensity factors at the crack tip are strongly affected by the behavior of the crack tip shape.

3.6 Effect of Local Damage

The complicated nature of fracture behavior in notched composite laminates makes it difficult to predict the exact position and size of every fiber break, matrix crack, and delamination even in a relatively simple notched panel studied here. The philosophy is not to model exactly, but to make approximations that agree well with actual behavior.

The objective of this section is to study the effect of damage in the vicinity of crack tip such as delamination and fiber splitting by comparing stress intensity factor computed using the three-dimensional FE analysis. It has been noted that for a tension loaded laminate, local damage is produced ahead of the crack tip in the form of the matrix cracks in off-axis plies, splitting in 0E plies and some delamination [11]. This local damage acts as a stress-relieving mechanism and relieves some portion of the high stress concentrated around the crack tip. This damage, such as matrix cracking and delamination, may significantly affect the structural integrity of the structures when they become sufficiently severe. However, failure models discussed in the previous section do not represent any effects of local damage. Axial splitting and delamination are the most common types of damage in laminated fiber reinforced composites due to their relatively

weak interlaminar strengths.

Previous finite element analysis used plane stress element in two-dimensional modeling. Therefore, the effect of delamination between plies in the thickness direction can not be modeled. In present finite element models, three-dimensional analysis was adopted to investigate the effect of delamination and axial splitting using twenty node, solid element (C3D20R element). Typically, solid element with reduced integration, is used to form the element stiffness for more accurate results and reduce running time. Sub-modeling analysis can be applied to shell-to-solid sub-model, however, the *z*-direction (thickness direction) stress and strain field can not be interpolated to 3D solid sub-model boundary from 2D global model. Thus, 3D global models were modeled to analyze 3D sub-model with local damage. Figure 3-26 shows the Von-Mises stress distribution in the $[0/\pm45]_s$ laminate of 3D global model and 3D sub-model. It should be noted that before interpolating the results of the 3D global model, the comparison between the results of 2D global model and 3D global model should be checked for consistent analysis. In Figure 3-27, the estimated stress intensity factors in the load-carrying ply from 3D global model are compared with those of 2D global model. The stress intensity factors obtained from 3D global model are slightly underestimated compared to those of the 2D global-model, however, these estimated values are fairly consistent for the nine laminate configurations. Consequently, two types of damage were modeled using 3D sub-model to predict the effect of local damage on the stress intensity factor of the load-carrying ply.

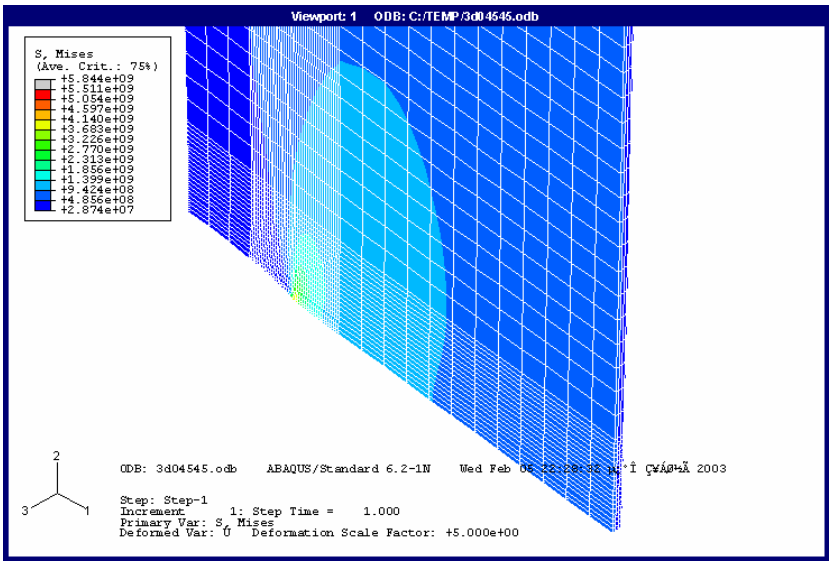

(a) 3D global model

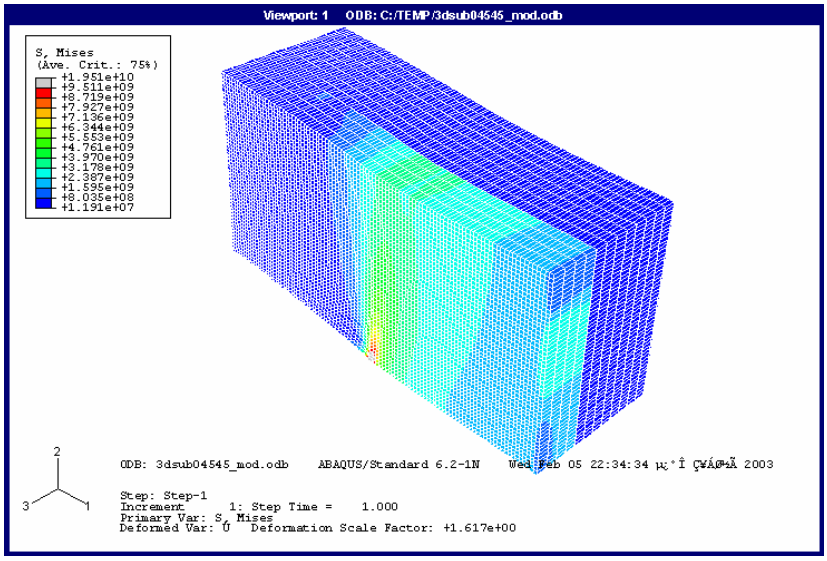

(b) 3D sub-model

Figure 3-26 Von-Mises stress distribution in $[0/"45]_s$ laminate

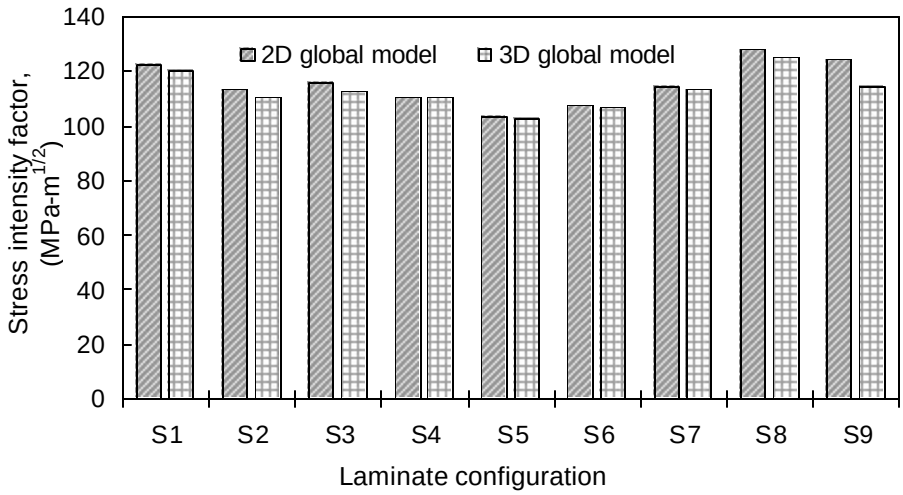

Figure 3- 27 Comparison of stress intensity factor of the load-carrying ply between 2D and 3D global model

3.6.1 3D FE Modeling Procedure for Delamination

All aspects of the finite element model were kept the same as 3D sub-model except interface of ply. Each ply was modeled by four elements through the thickness as shown in Figure 3-26(b). Elements of layers are connected through either side of any ply interfaces at common nodes except where delamination is expected. The delamination was modeled as separate, unconnected nodes with identical coordinates. Figure 3-28 show the schematic of ply interface mesh where delamination is expected. To estimate delamination area, a simple delamination criterion was implemented in ABAQUS by means of a UVAR user subroutine using the following equation.

$$\text{Delamination area}: \sqrt{t_{xz}^2 + t_{yz}^2 + s_{zz}^2} \le S_T \qquad (22)$$

where S_T is critical stress of matrix which is 75 MPa based on typical epoxy yield strength. Figure 3- 29 shows the estimated delamination area using the above

delamination criterion in the ply between the load-carrying ply and +45E ply of $[0/\pm45]_s$ laminate.

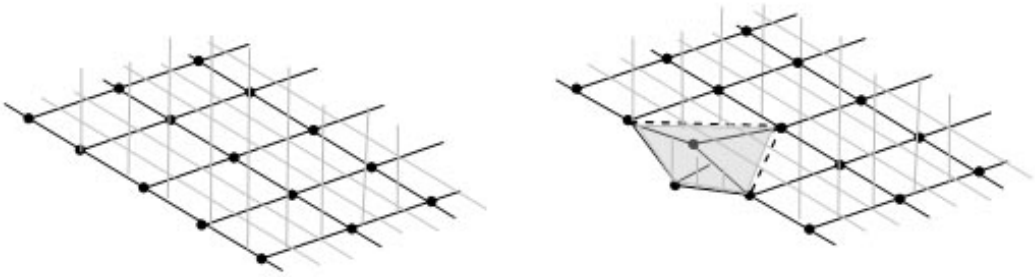

(a) no damage (b) delamination

Figure 3-28 Scheme of ply interface mesh in the $[0/\pm45]_s$ laminate

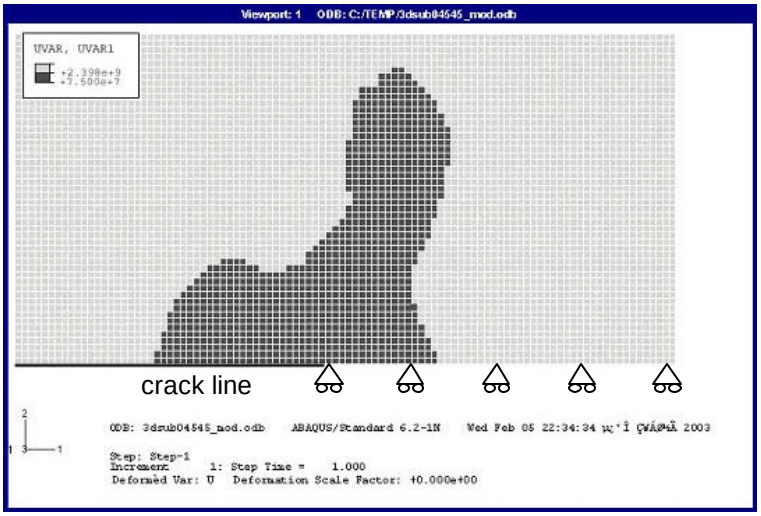

Figure 3-29 Estimated delamination area on interface between 0E and +45E ply in the $[0/\pm45]_s$ laminate

3.6.2 3D FE Modeling Procedure for Axial Splitting

When a notched composite panel is subjected to tension loading axial splitting occurs in the crack tip area due to high stress concentration and low matrix tensile strength. Apparently, this failure mode causes severe stiffness reduction in transverse direction. Thus, transverse stiffness of axial splitting area can be modeled by taking $E_T \approx 0$. This failure mode and assumption are illustrated in Figure 3-30. Similar method described in the previous section was used to estimate axial splitting area where reduced stiffness property was implemented, E_T=10 Pa that is extremely small compared to initial modulus, E_T=9.65 GPa. A critical stress of 75 MPa was used, based on a typical epoxy yield stress. Figure 3-31 shows the estimated axial splitting area in the interface between 0E and +45E ply for a tensile loading 351.14 MPa.

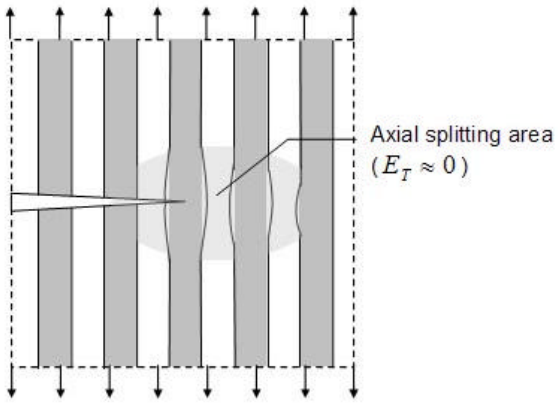

Figure 3-30 Axial splitting failure mode in the load-carrying ply

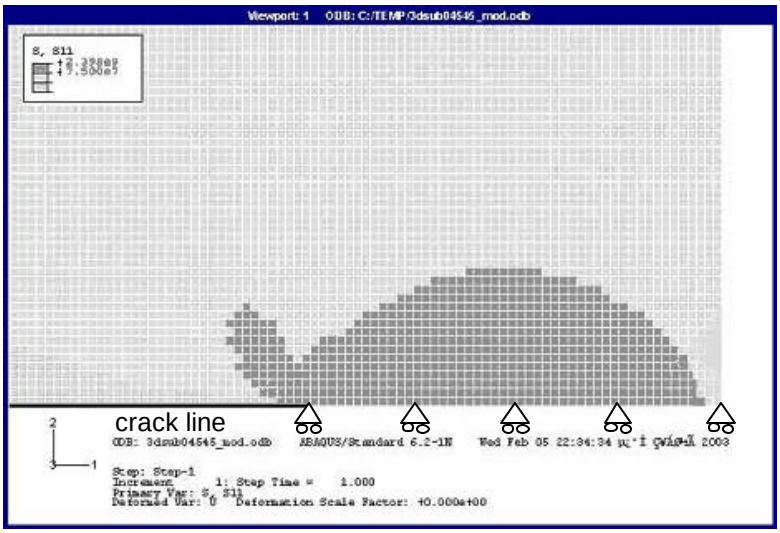

Figure 3-31 Estimated axial splitting area on interface between 0E and +45E ply

3.6.3 Results and Discussion

Typical damage in notched laminated composites occurs in the form of axial splitting in the load-carrying ply and delamination. This damage was modeled to study effect of local damage on the normal stress distribution in the vicinity of crack tip in the load-carrying ply. The estimated delamination area and axial splitting area are modeled by having duplicate nodes and reduced stiffness, respectively.

Results of normal stress distribution are shown in Figure 3-32. From the results it is observed that s_y distribution in the FE model without damage shows the typical square root singularity. Axial splitting and delamination removes the singularity, though there still is a region of high stress concentration near the crack tip. It also can be seen that s_y distribution increases away from the crack tip and s_x distribution in the model with damage decreases than in the model with no damage. Thus, the stress field is strongly affected by the presence of local damage. From the results, it is obvious that the local

damage serve as main mechanism to increase s_y distribution and decreases s_x distribution in the load-carrying ply. This simulation is similar to the redistribution of stress in the presence of small scale yielding in homogenous materials.

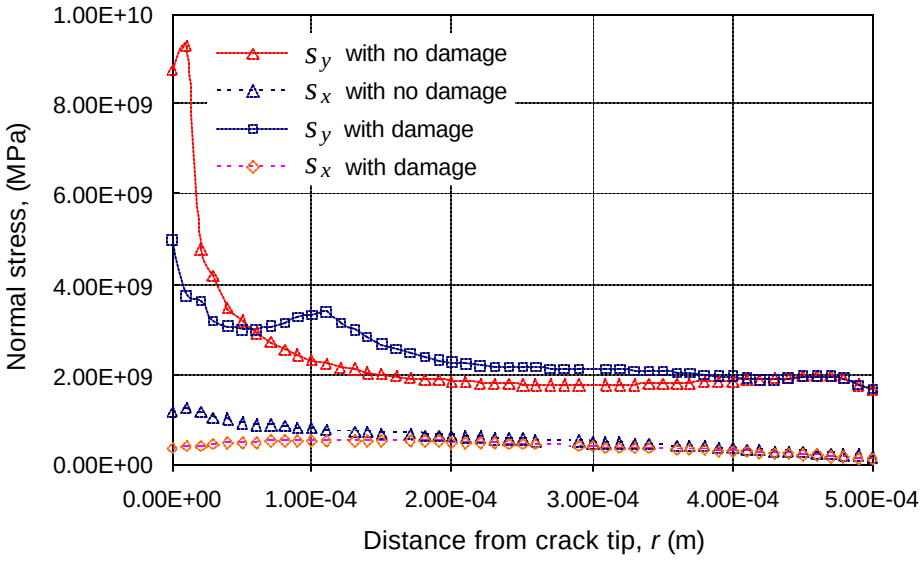

Figure 3-32 Effect of the local damage on normal stress distribution in the load-carrying ply in the $[0/\pm45]_s$ laminate

3.7 Summary of FE Results and Discussion

It is well established that the fracture behavior of composite laminates depends on a variety of variables. All may affect to varying degrees the fracture behavior of the notched laminates. A comprehensive evaluation is still lacking regarding the effects of all variables on the notch sensitivity of composite laminates. Through the detailed finite element analysis, we investigated effect of distinct factors such as crack tip shape and local damage.

The presence of blunt crack tip has a significant effect on the behavior of notched composites, and leads to stress redistribution. This relives the stresses in the non-load-carrying plies and increases the SIF of the load-carrying plies. Similar effects are observed when local damage such as matrix cracking and delamination are introduced.

Figure 3-33 shows the results of finite element sub-model, which include blunt crack tip and local damage. From the comparison of the results between models with and without damage, it is obvious that these effects also increase the stress intensity factor of the load-carrying ply as a result of the reduction in s_x stress concentration in the laminate. By comparing the results of finite element analysis with analytical failure model, it can be reasonably assumed that the effect of initial damage is accounted by reducing the s_x component ahead of crack tip to zero.

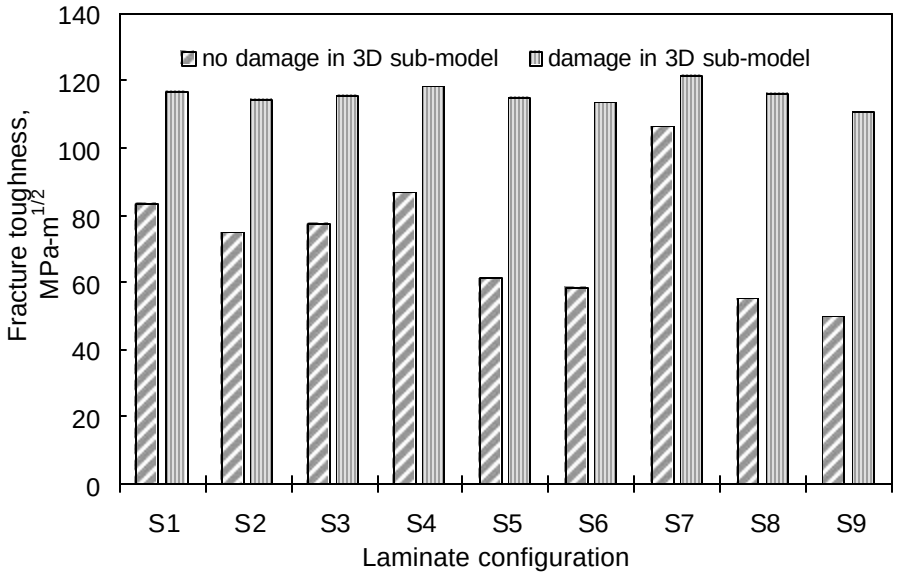

Figure 3-33 Effect of the local damage on stress intensity factor in the load-carrying ply

CHAPTER 4
CONCLUSIONS AND FUTURE WORK

CONCLUSIONS

The SIF of the load-carrying ply is a critical parameter for predicting the failure of notched composite laminates. The SIF of the load-carrying ply, K_Q^L, can be estimated by using a detailed 3D FE analysis which can model local damage modes such as fiber splitting and delamination that occurs prior to fracture. Then the SIF of the load-carrying ply can be calculated accurately and compared with the critical value for the material system to predict fracture. The results from this model are presented in Column 2 of Table 4-1.

On the other hand, a simpler analytical model could be used. In this model finite-width correction factor for orthotropic laminates should be used. The effects of local damage at the crack tip is accounted for by setting the parameter b=0 in Eq. (15) for calculating the SIF of the load-carrying ply. Results from such analysis are shown in Column 3 of Table 4-1. The results from calculations performed by Sun and Vaiday [11] are given in Column 4 for comparison.

Using a mean value of 113.81 MPa-$m^{1/2}$ for K_Q^L in the analytical model, the predictions of the laminate fracture toughness are compared with the experimental results in Figure 4-2 for various value of h.

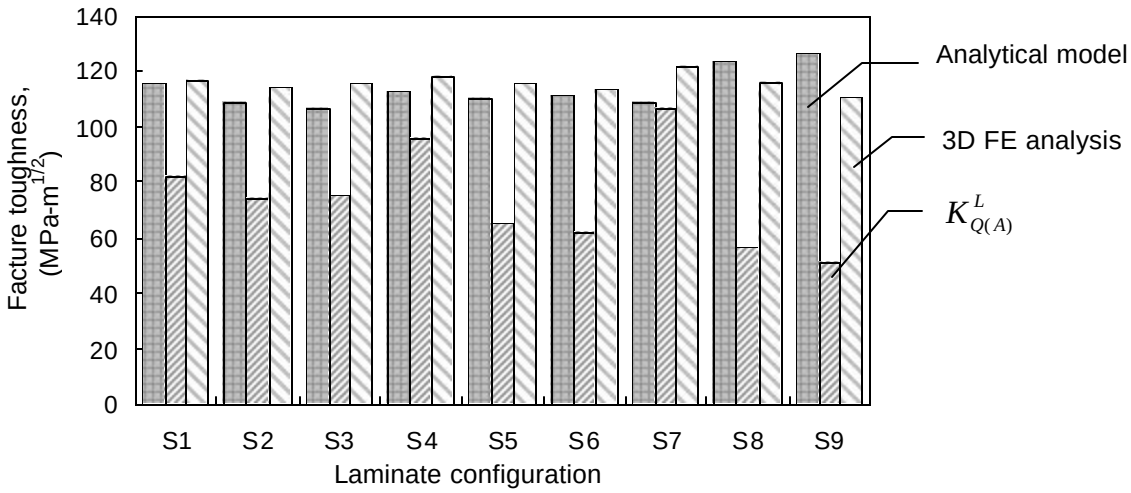

Figure 4-1 Comparison of the fracture toughness of load-carrying ply

Table 4-1 Comparison of the fracture toughness of load-carrying ply obtained from different methods

Specimen	Fracture toughness of load-carrying ply, K_Q^L, MPa-m$^{1/2}$		
	3D FE analysis	Analytical model	Ref. [11]
S1	116.65	115.66	115.66
S2	114.23	108.82	108.82
S3	115.71	106.43	106.43
S4	118.16	112.62	101.81
S5	115.21	109.97	101.00
S6	113.53	111.52	106.32
S7	121.40	109.04	109.04
S8	116.01	123.66	119.81
S9	110.51	126.58	123.64
average	115.71	113.81	110.28
S.D.†	3.03 %	6.95 %	9.80 %

† standard deviation

The variable h was defined as ratio of stress intensity factor of the load-carrying ply to that of laminate and can be obtained from Eq. (15). It should be noted that ?, like ß, depends entirely on the laminate properties. Good agreement is observed between the experiments and predictions. By comparison with experimental results, it is concluded that the proposed lay-up independent model with orthotropic finite-width correction factor is capable of predicting fracture toughness of notched laminated composites with reasonable accuracy for mode I loading.

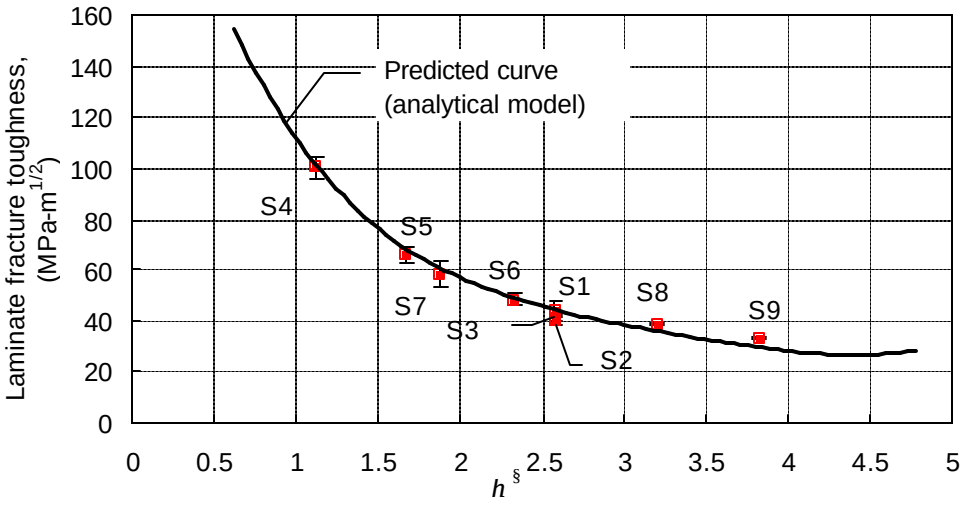

§ h is defined as $h = \frac{K^{L}_{Q(B)}}{K_Q} = t\left[\overline{Q}^{L}_{12}A^{*}_{12} + \overline{Q}^{L}_{22}A^{*}_{22}\right]$ from Eq. (15)

Figure 4-2 Comparison of experimental results with failure model predictions

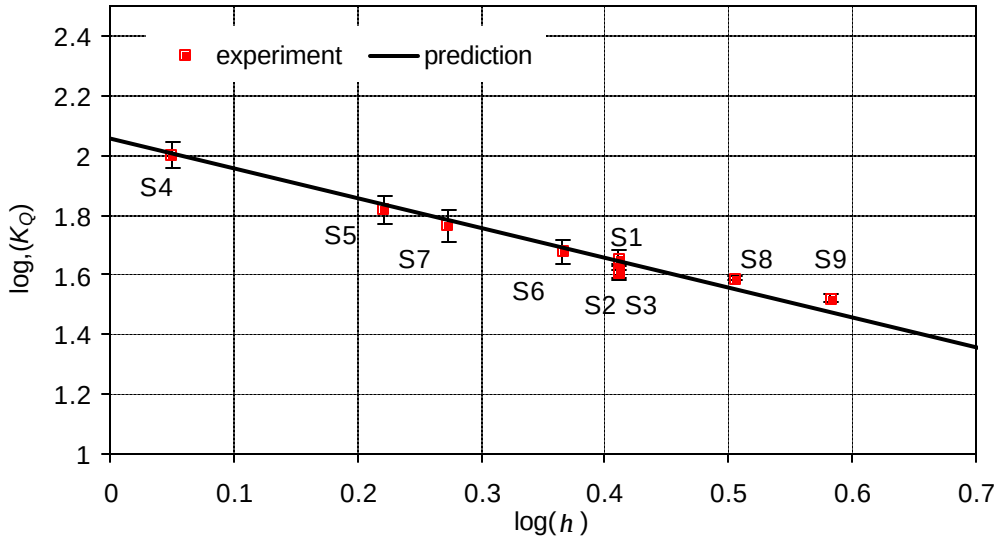

Figure 4-3 Comparison of experimental results with failure model predictions (log scale)

Table 4-2 Comparison of experimental results with failure model predictions

Specimen		h	Fracture toughness of laminates, K_Q (MPa-m$^{1/2}$)		
Notation	Lay-up		Experiment†	Prediction‡	Relative error (%)
S1	$[0/90/\pm45]_s$	2.5791	44.67768	44.1295	1.23
S2	$[\pm45/90/0]_s$	2.5791	40.22554	44.1295	-9.71
S3	$[90/0/\pm45]_s$	2.5791	41.16729	44.1295	-7.20
S4	$[0/\pm15]_s$	1.1209	100.4675	101.5384	-1.07
S5	$[0/\pm30]_s$	1.6619	66.24291	68.48451	-3.38
S6	$[0/\pm45]_s$	2.3215	48.07307	49.02623	-1.98
S7	$[0/90]_{2s}$	1.8706	58.19245	60.84379	-4.56
S8	$[\pm45/0/\pm45]_s$	3.1979	38.68474	35.59036	7.99
S9	$[\pm452/0/\pm45]_s$	3.8168	33.19171	29.81933	10.16

† Fracture toughness of laminates obtained using Eq. (1) with orthotropic finite-width correction factor in Table 3-4.

‡ Predicted fracture toughness of laminates calculated using the mean value, 113.81 MPa-m$^{1/2}$, for K_Q^L in the analytical model.

FUTURE WORK

There seems to be ample room for further investigation of this problem. Fracture problem studied in the current study was limited to AS4/3501-6 graphite/epoxy laminated panel containing a center straight crack subjected to tension loading. For general application, validity of currently proposed lay-up independent criterion can be further verified for the case of laminated composite panels containing double edge notch, single edge notch, circular hole, etc. with different material systems using experimental and numerical analyses for mode II and mixed loading conditions. Additionally, this failure model can be compared with other popular failure models such as Point Stress Criterion, Average Stress Criterion, Mar-Lin failure model, etc. so that composite structure designers can select an appropriate failure model in diverse practical situations.

APPENDIX A
LAMINATION THEORY

For laminated plates with bending-extension coupling under plane stress, the complete set of force-mid-plane deformation equations can be expressed in matrix form as

$$\left\{\frac{N}{M}\right\}=\left[\frac{A\,|\,B}{B\,|\,D}\right]\left\{\frac{e^0}{k}\right\} \tag{A-1}$$

where N and M are the in-plane forces and moments, respectively, and e^0 is the mid-plane strains, and k is the curvature.

In the case of symmetric laminates without coupling, Eq. (A-1) is reduced to

$$\begin{Bmatrix} N_x \\ N_y \\ N_{zy} \end{Bmatrix}=\begin{bmatrix} A_{11} & A_{12} & A_{16} \\ A_{12} & A_{22} & A_{26} \\ A_{16} & A_{26} & A_{66} \end{bmatrix}\begin{Bmatrix} e_x^0 \\ e_y^0 \\ g_{xy}^0 \end{Bmatrix} \tag{A-2}$$

where the laminate extensional stiffness are given by

$$A_{ij}=\int_{-t/2}^{t/2}(\overline{Q}_{ij})_k\,dz \tag{A-3}$$

where t is the thickness of the laminate. If there are N layers in the lay-up, we can rewrite the above equations as a summation of integrals over the laminate. The material coefficients will then take the form

$$A_{ij}=\sum_{k=1}^{N}(\overline{Q}_{ij})_k(z_k-z_{k-1}) \tag{A-4}$$

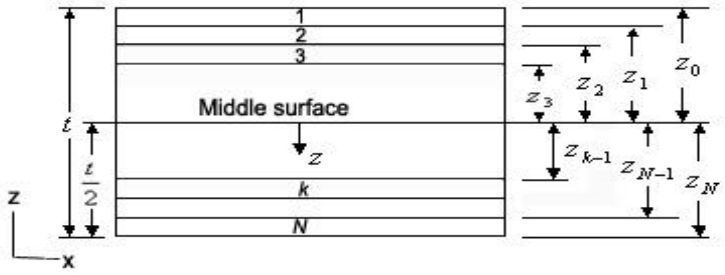

Figure A-1 Laminated plate geometry

where the z_k and z_{k-1} in these equation indicate that the k^{th} lamina is bounded by surfaces z_k and z_{k-1}. Thus, the $\overline{Q}_{ij}$ depend on the material properties and fiber orientation of the k^{th} layer. It can be obtained using the following equation.

$$[\overline{Q}] = [T^{-1}]\,[Q]\,[R]\,[T]\,[R^{-1}] \tag{A-5}$$

where

$$[T] = \begin{bmatrix} m^2 & n^2 & mn \\ n^2 & m^2 & -mn \\ -2mn & 2mn & m^2 - n^2 \end{bmatrix}, \qquad [R] = \begin{bmatrix} 1 & 0 & 0 \\ 0 & 1 & 0 \\ 0 & 0 & 2 \end{bmatrix} \tag{A-6}$$

$$m = \cos q \quad \text{and} \quad n = \sin q$$

where the $\overline{Q}_{ij}$ are the components of the transformed lamina stiffness matrix which are defined as follows

$$\begin{aligned}
\overline{Q}_{11} &= Q_{11}\cos^4 q + Q_{22}\sin^4 q + 2(Q_{12} + 2Q_{66})\sin^2 q \cos^2 q \\
\overline{Q}_{12} &= (Q_{11} + Q_{22} - 4Q_{66})\sin^2 q \cos^2 q + Q_{12}(\sin^4 q + \cos^4 q) \\
\overline{Q}_{22} &= Q_{11}\sin^4 q + Q_{22}\cos^4 q + 2(Q_{12} + 2Q_{66})\sin^2 q \cos^2 q \\
\overline{Q}_{16} &= (Q_{11} - Q_{12} - 2Q_{66})\sin q \cos^3 q + (Q_{12} - Q_{22} + 2Q_{66})\sin^3 q \cos q \\
\overline{Q}_{26} &= (Q_{11} - Q_{12} - 2Q_{66})\sin^3 q \cos q + (Q_{12} - Q_{22} + 2Q_{66})\sin q \cos^3 q \\
\overline{Q}_{66} &= (Q_{11} + Q_{12} - 2Q_{12} - 2Q_{66})\sin^2 q \cos^2 q + Q_{66}(\sin^4 q + \cos^4 q)
\end{aligned} \tag{A-7}$$

$$\begin{Bmatrix} e_x^0 \\ e_y^0 \\ g_{xy}^0 \end{Bmatrix} = \begin{bmatrix} A_{11}^* & A_{12}^* & A_{16}^* \\ A_{12}^* & A_{22}^* & A_{26}^* \\ A_{16}^* & A_{26}^* & A_{66}^* \end{bmatrix} \begin{Bmatrix} N_x \\ N_y \\ N_{zy} \end{Bmatrix} \tag{A-8}$$

where superscript * denotes the component of inverse matrix of $[A]$

The stresses in each ply can be recovered form the mid-plane strains. In particular, the stresses in the load-carrying ply can be expressed as

$$\begin{Bmatrix} s_x^L \\ s_y^L \\ t_{xy}^L \end{Bmatrix} = \begin{bmatrix} \overline{Q}_{11}^L & \overline{Q}_{12}^L & \overline{Q}_{16}^L \\ \overline{Q}_{12}^L & \overline{Q}_{22}^L & \overline{Q}_{26}^L \\ \overline{Q}_{16}^L & \overline{Q}_{26}^L & \overline{Q}_{66}^L \end{bmatrix} \begin{Bmatrix} e_x^0 \\ e_y^0 \\ g_{xy}^0 \end{Bmatrix} \tag{A-9}$$

where superscript ^{L} means the component of principal load carrying ply

The normal stress field applied in the load-carrying ply can be obtained by calculating the portion of the applied load that is carried by the load-carrying ply using lamination theory using Eqs. (A-8) and (A-9).

$$\begin{Bmatrix} s_x^L \\ s_y^L \\ t_{xy}^L \end{Bmatrix} = \begin{bmatrix} \overline{Q_{11}^L} & \overline{Q_{12}^L} & \overline{Q_{16}^L} \\ \overline{Q_{12}^L} & \overline{Q_{22}^L} & \overline{Q_{26}^L} \\ \overline{Q_{16}^L} & \overline{Q_{26}^L} & \overline{Q_{66}^L} \end{bmatrix} \begin{bmatrix} A_{11}^* & A_{12}^* & A_{16}^* \\ A_{12}^* & A_{22}^* & A_{26}^* \\ A_{16}^* & A_{26}^* & A_{66}^* \end{bmatrix} \begin{Bmatrix} N_x \\ N_y \\ N_{xy} \end{Bmatrix} \tag{A-10}$$

APPENDIX B
MATHEMATICAL THEORIES OF BRITTLE FRACTURE

The objective of this Appendix was to provide the brief review of mathematical formulation of crack problems for derivation of stress intensity factor in homogeneous orthotropic materials [17].

For orthotropic materials in the case of plane stress, the generalized Hooke law can be expressed as

$$\begin{aligned} e_{xx} &= a_{11}s_{xx} + a_{12}s_{yy} + a_{16}t_{xy} \\ e_{yy} &= a_{12}s_{xx} + a_{22}s_{yy} + a_{26}t_{xy} \\ g_{xy} &= a_{16}s_{xx} + a_{26}s_{yy} + a_{66}t_{xy} \end{aligned} \tag{B-1}$$

$$s_{xz} = s_{yz} = s_{z} = 0$$

The equilibrium equations under plane stress conditions are

$$\frac{\partial s_{xx}}{\partial x} + \frac{\partial t_{xy}}{\partial y} = 0, \qquad \frac{\partial t_{yx}}{\partial x} + \frac{\partial s_{yy}}{\partial y} = 0 \tag{B-2}$$

The equilibrium equations will be satisfied if the stress function *U(x,y)* is expressed as

$$s_{xx} = \frac{\partial^2 U}{\partial y^2}, \qquad s_{yy} = \frac{\partial^2 U}{\partial x^2}, \qquad t_{xy} = -\frac{\partial^2 U}{\partial y \partial x} \tag{B-3}$$

Substituting for s_{xx}, s_{yy}, t_{xy} from Eq. (B-3) in the compatibility equation

$$\frac{\partial^2 e_{xx}}{\partial y^2} + \frac{\partial^2 e_{yy}}{\partial x^2} = \frac{\partial g_{xy}}{\partial x \partial y} \tag{B-4}$$

The governing characteristic equation of plane stress of orthotropic materials can be expressed as

$$a_{22}\frac{\partial^4 U}{\partial x^4} - 2a_{26}\frac{\partial^4 U}{\partial x^3 \partial y^2} + (2a_{12} + a_{66})\frac{\partial^4 U}{\partial x^2 \partial y^2} - 2a_{16}\frac{\partial^4 U}{\partial x \partial y^3} + a_{11}\frac{\partial^4 U}{\partial y^4} = 0 \qquad \text{(B-5)}$$

Defining the operators D_j (j= 1, 2, 3, 4) as

$$D_j = \frac{\partial}{\partial y} - m_j \frac{\partial}{\partial x} \quad (j\text{= 1, 2, 3, 4}) \qquad \text{(B-6)}$$

The governing equation in $U(x,y)$ becomes

$$D_1 D_2 D_3 D_4 U(x,y) = 0 \qquad \text{(B-7)}$$

and m_j are the roots of the characteristic equation.

$$a_{11}m_j^4 - 2a_{16}m_j^3 + (2a_{12} + a_{66})m_j^2 - 2a_{26}m_j + a_{22} = 0 \qquad \text{(B-8)}$$

The roots are either complex or purely imaginary and cannot be real and can be expressed as

$$s_1 = m_1 = a_1 + id_1, \qquad s_2 = m_2 = a_2 + id_2,$$
$$u_3 = \bar{u}_1, \qquad u_4 = \bar{u}_2 \qquad \text{(B-9)}$$

where a_i, d_j $(j= 1, 2)$ are real constants.

The stress function $U(x,y)$ can be expressed in the form

$$U(x,y)=2\,Re\,[U_1(z_1)+U_2(z_2)] \qquad \text{(B-10)}$$

where $U_1(z_1)$ and $U_2(z_2)$ are the arbitrary functions of the complex variables $z_1 = x + s_1 y$ and $z_2 = x + s_2 y$, respectively. Let new functions

$$f(z_1) = dU_1/dz_1, \quad y(z_2) = dU_2/dz_2 \qquad \text{(B-11)}$$

Substituting the stress function from Eq. (B-10) into the Eq. (B-3) and taking into account the relations in Eq. (B-11), the stress components can be expressed as

$$
\begin{aligned}
s_x &= 2\,\mathrm{Re}[s_1^2 2f'(z_1) + s_2^2 2y'(z_2)] \\
s_y &= 2\,\mathrm{Re}[f'(z_1) + y'(z_2)] \\
t_{xy} &= -2\,\mathrm{Re}[s_1 f'(z_1) + s_2 y'(z_2)]
\end{aligned}
\tag{B-12}
$$

For pure mode I case, the stress components in the vicinity of crack tip can be expressed in terms of stress intensity factor, K_I, and the roots of characteristic Eq. (B-8)

$$
\begin{aligned}
s_y &= \frac{K_I}{\sqrt{2pr}}\,\mathrm{Re}\left[\frac{1}{s_1 - s_2}\left(\frac{s_1}{\sqrt{\cos q + s_2 \sin q}} - \frac{s_2}{\sqrt{\cos q + s_1 \sin q}}\right)\right] \\
s_x &= \frac{K_I}{\sqrt{2pr}}\,\mathrm{Re}\left[\frac{s_1 s_2}{s_1 - s_2}\left(\frac{s_2}{\sqrt{\cos q + s_2 \sin q}} - \frac{s_1}{\sqrt{\cos q + s_1 \sin q}}\right)\right] \\
t_{xy} &= \frac{K_I}{\sqrt{2pr}}\,\mathrm{Re}\left[\frac{s_1 s_2}{s_1 - s_2}\left(\frac{1}{\sqrt{\cos q + s_1 \sin q}} - \frac{1}{\sqrt{\cos q + s_2 \sin q}}\right)\right]
\end{aligned}
\tag{B-13}
$$

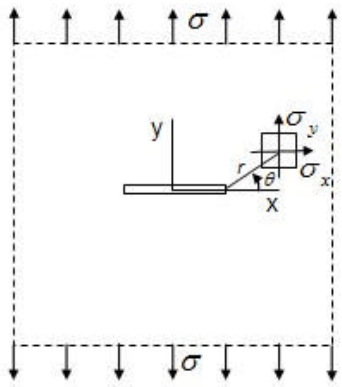

Figure B-1 Stress components in the vicinity of crack tip

when q = 0, the new parameter ß introduced in the Chapter 2.3 can be expressed as (

$$
b = \frac{s_x(r,0)}{s_y(r,0)} = \mathrm{Re}\left[-s_1 s_2\right] \tag{B-14}
$$

Consequently, the model I stress intensity factor can be expressed as

$$
K_I = \lim_{r \to 0} s_y(r,0)\sqrt{2pr} \tag{B-15}
$$

K_I can also be expressed in terms of s_x as

$$K_I = \frac{\lim_{r\to 0} s_x(r,0)\sqrt{2pr}}{b} \tag{B-16}$$

The increase in strain energy due to the presence of the crack can be calculated using following equation for mode I case.

$$\Delta W = \frac{1}{2}\int_{-a}^{a} s_{yy}(x,0)\Delta u_y dx \tag{B-17}$$

The derivative of ΔW with respect to crack size, a, yield

$$\frac{\partial \Delta W}{\partial a} = K_I^2 a_{22}\,\mathrm{Re}\left[i\left(\frac{s_1+s_2}{s_1 s_2}\right)\right] \tag{B-18}$$

The energy release rate can be expressed in terms of stress intensity factor

$$G_I = \frac{K_I^2}{2} a_{22}\,\mathrm{Re}\left[i\left(\frac{s_1+s_2}{s_1 s_2}\right)\right] \tag{B-19}$$

where $s_i\,(j = 1,2)$ are the roots of the characteristic equation (B-8) which can be derived from the elastic constants as

$$s_1 s_2 = -\left(\frac{a_{22}}{a_{11}}\right)^{1/2}, \qquad s_1 + s_2 = i\sqrt{2}\left[\left(\frac{a_{22}}{a_{11}}\right)^{1/2} + \left(\frac{2a_{12}+a_{66}}{2a_{11}}\right)\right]^{1/2} \tag{B-20}$$

Then, the relation equation between G_I and K_I for an orthotropic material can be expressed as

$$G_I = K_I^2\left(\frac{a_{11}a_{22}}{2}\right)^{1/2}\left[\left(\frac{a_{22}}{a_{11}}\right)^{1/2} + \frac{2a_{12}+a_{66}}{2a_{11}}\right]^{1/2} \tag{B-21}$$

LIST OF REFERENCES

[1] Awerbuch J, Madhukar M.S., "Notched strength of composite laminates: prediction and experiments-a review." Journal of Reinforced Plastics and Composites 1985;4:3-159

[2] Waddoups M.E., Eisenmann J.R., Kaminski B.E., "Macroscopic fracture mechanics of advanced composites materials." Journal of Composites Materials 1971;5:446-54

[3] Whitney J.M., Nuismer R.J., "Stress fracture criteria for laminated composites containing concentrations." Journal of Composite Materials 1974;8:253-65.

[4] Tan S.C., "Effective stress fracture models for unnotched and notched multidirectional laminates." Journal of Composites Material 1988;22:322-40.

[5] Mar L.W., Lin K.Y., "Fracture mechanics correlation for tensile failure of filamentary composites with holes." Journal of Aircraft 1977;14:703-707

[6] Chang F.K., Chang K.Y., "Progressive damage model for laminated composites containing stress concentration." Journal of Composites Materials 1987;21:834-855

[7] Tan S.C., "A progressive failure model for composite laminates containing openings." Journal of Composites Materials 1991;25:556-577

[8] Poe C.C. Jr., "An unified strain criterion of fracture of fibrous composite laminates." Engineering Fracture Mechanics 1983;17:153-171

[9] Poe C.C. Jr., Sova J.A., "Fracture toughness of boron/aluminum laminates with various proportions of 0E and ±45Eplies." NASA Technical Paper 1707. Nov 1980

[10] Kageyama K., "Fracture mechanics of notched composite laminates." Application of Fracture Mechanics to Composites Materials 1989;327-396

[11] Sun C.T., Vaiday R.S., "Fracture criterion for notched thin composite laminates." AIAA Journal 1998;36:81-8.

[12] Sun C.T., Vaiday R.S., Klug J.C., "Effect of ply thickness on fracture of notched composite laminates." AIAA Journal 1988;36:81-8.

[13] Tan S.C., "Finite-width correction factors for anisotropic plate containing a central opening." Journal of Composite Materials 1998;22:1080-1098

[14] Naik N.K., Shembekar P.S., "Notched strength of fabric laminates." Composites Science and Technology 1992;44:1-12.

[15] Gillespie, J.W. Jr., Carlsson L.A., "Influence of finite width on notched laminate strength predictions." Composites Science and Technology 1988;32:15-30

[16] Wisnom M.R., Chang F.K., "Modeling of splitting and delamination in notched cross-ply laminates." Composites Science and Technology 2000;60:2849-2856

[17] Sih G.C., Liebowitz H., Fracture and an Advanced Treatise. Volume II Mathematical Fundamentals edited by Liebowitz H. 1968, Academic Press, New York and London

[18] Hibbit, Karlsson, Sorensen, ABAQUS version 6.2 Theory Manual published by Hibbit, Karlsson & Sorensen, Inc. 1998, U.S.A.

BIOGRAPHICAL SKETCH

Bokwon Lee was born on July 15, 1973, in Kyungki province, Republic of Korea, as the second son of Jonghan Lee and Jongok Woo. He graduated from Korea Airforce Academy with a B.S. degree in aeronautical engineering in March 1996. After graduation, He worked at the 19th Fighter Wing, Jungwon, Republic of Korea, for 3 years. After promotion to Captain, he worked for Airforce Logistics Command as a technical assistant for tactical combat aircrafts.

He came to the University of Florida for his graduate study in August 2001 and began his research with Dr. Bhavani V. Sankar in the Department of Mechanical and Aerospace Engineering. He completed his master's program in August 2003.